Universitat d'Alacant
Universidad de Alicante
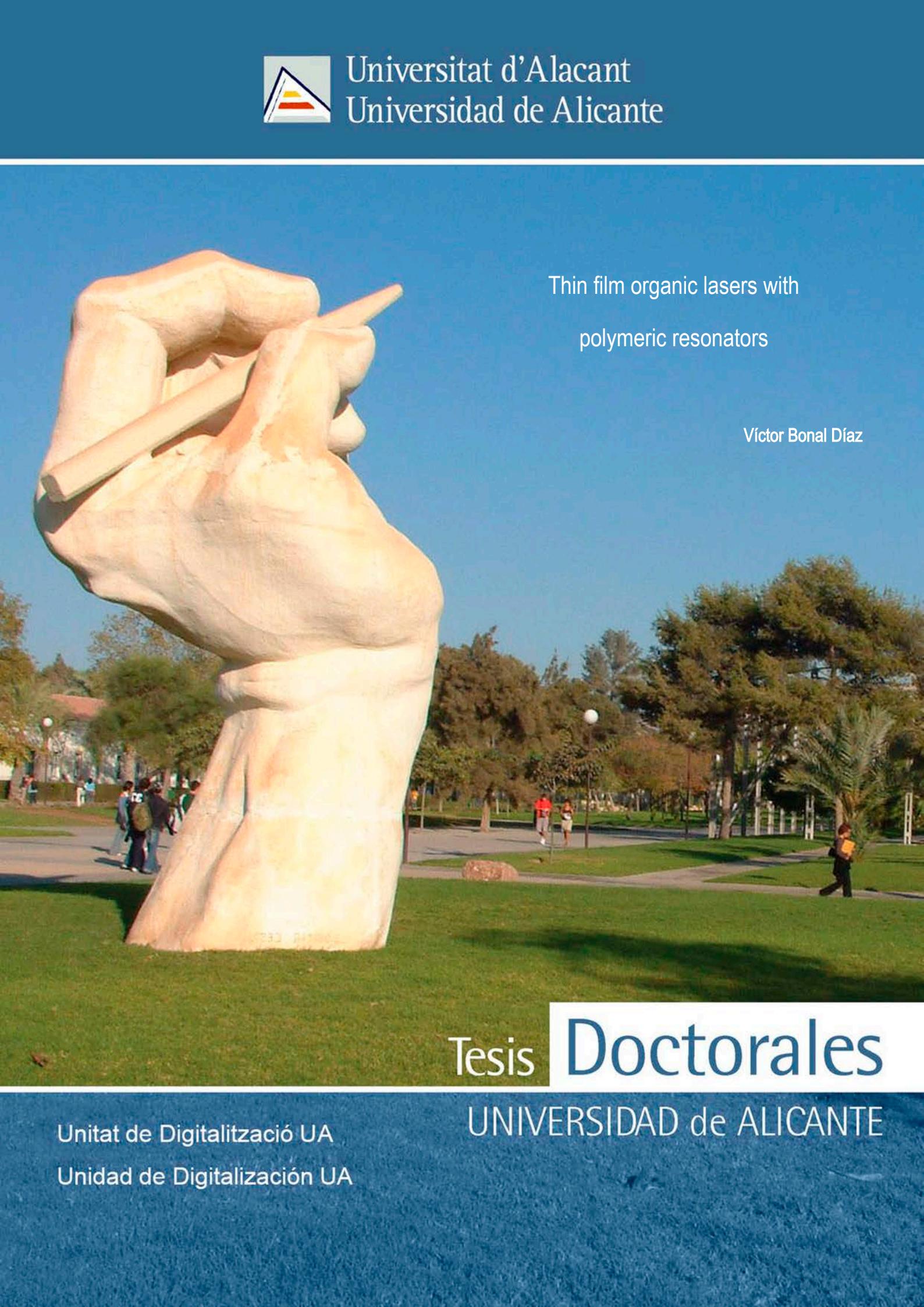
Thin film organic lasers with

polymeric resonators

Víctor Bonal Díaz

Tesis **Doctorales**

UNIVERSIDAD de ALICANTE

Departamento de Física Aplicada

Instituto Universitario de Materiales

Facultad de Ciencias

Thin film organic lasers with polymeric resonators

Víctor Bonal Díaz

Tesis presentada para aspirar al grado de

DOCTOR POR LA UNIVERSIDAD DE ALICANTE

MENCIÓN DE DOCTOR INTERNACIONAL

DOCTORADO EN CIENCIA DE MATERIALES

Dirigida por

Prof. María Ángeles Díaz García

Catedrática de la Universidad de Alicante

Alicante, septiembre 2022

No faces de la teua ignorància un argument.

Joan Fuster

A mis abuelos, especialmente
a mi yaya Carmen y a mi yayo Marcelino.

Agradecimientos

En primer lugar, quiero dar las gracias a María Díaz García, por la oportunidad de realizar esta tesis doctoral y por todo el apoyo y consejo recibido durante esta etapa, que sin duda me acompañarán durante toda mi vida. No podía faltar el agradecimiento a Pedro Boj, José Antonio Quintana y Moisés Villalvilla, que desde el primer momento me acogieron en el grupo de investigación y que tanto me han ayudado y enseñado en todos los momentos compartidos en el laboratorio. Gracias por mostrarme de primera mano y día a día el mejor ejemplo de lo que debe ser un científico y una gran persona.

Siempre viene bien compartir las experiencias y tener a alguien un poco adelantado en el camino para que te pueda servir de guía. No me podría haber tocado mejor compañero para vivir esta etapa que Rafa Muñoz. Muchas gracias por enseñarme los entresijos del laboratorio y por estar siempre dispuesto a ayudar con lo que hiciese falta con la mejor de las actitudes. También quiero dar las gracias a Eva Calzado, Manuel Gutiérrez, Víctor Navarro y Marta Morales, que también obtuvieron el doctorado en el grupo de investigación de electrónica y fotónica orgánicas. La investigación siempre se basa en trabajos y desarrollos anteriores, así que esta tesis está sustentada también por el trabajo previo que realizaron en este laboratorio. Además, he tenido la suerte de conocerlos personalmente e incluso colaborar con ellos, así que no tengo más que palabras de agradecimiento hacia todos ellos por la ayuda recibida. Gracias también a todas las personas que han ido pasando por el laboratorio a lo largo del tiempo que he estado aquí y especialmente a Jose Carlos Mira, compañero de fatigas durante el final de esta etapa y que tanto me ha ayudado.

Gracias al Prof. Uli Lemmer por la oportunidad de realizar una estancia en su grupo de investigación en el Karlsruhe Institute of Technology de Alemania y a Isabel Allegro por toda la ayuda recibida durante la estancia, tanto en el ámbito científico como en el personal. Y gracias a todos los colaboradores que han hecho posible esta tesis.

No pueden faltar las gracias a todos mis amigos que han estado ahí durante este proceso, tanto los de toda la vida como los nuevos amigos que he hecho durante mi etapa en la Universidad de Alicante. Y por supuesto a mi familia, a la que les debo todo y que de la que estoy muy orgulloso, con especial cariño a mis padres y mi hermana Marina. Por último, gracias a Gema por animarme y apoyarme siempre y por estar siempre a mi lado.

Abstract

Distributed feedback lasers (DFB) are some of the most studied thin film organic lasers, as they are cost-efficient, compact, and can be easily integrated with other devices. Besides, they are useful for a wide range of applications, such as spectroscopy, optical communications, and sensing. An organic DFB laser typically consists of an organic active thin film deposited over a relief grating engraved in an inorganic substrate (standard configuration), but it can present different architectures depending on the position of the resonator and the materials used for its fabrication. Here, a DFB laser architecture with a polymeric resonator deposited on top of the active film is studied. This architecture offers several advantages over the standard one. The device is easier to fabricate, as both films are organic and solution- processable, the active film presents a uniform thickness, and the grating period can be easily adjusted for each case as it is fabricated using holographic lithography.

In this thesis, the optimization of DFB lasers based on polymeric diffractive resonators located on top of the active films has been achieved following two different goals: the resonator optimization through the control of the fabrication and the geometrical parameters; and the design and fabrication of optimized DFB lasers for new organic molecules to be used as active materials. The first step in the resonator optimization was to perform a systematic study of the effect of the fabrication process parameters on the final resonator characteristics in devices emitting in the visible, analyzing the influence of these parameters on the final DFB lasers emission properties. After that, the capability of the material used for the grating fabrication (dichromated gelatin, DCG) to form part of DFB lasers emitting at lower wavelengths (blue and deep-blue) was examined. Lastly, the DFB laser architecture with the resonator on top of the active film was compared to the standard configuration under variables not considered yet (such as the use of a dye which can be doped at high concentrations into the matrix, thus providing a way to change the refractive index of the active film) to prove its enhanced performance. Additionally, the whole fabrication process was upgraded with the study an implementation of a simple spectrophotometric method to measure the thickness and refractive index of polymeric thin films, which allows a better overall optimization of the devices. After the resonator optimization was fulfilled, DFB laser devices were fabricated and adapted to suit different active materials. Various families of novel compounds have been investigated with emissions from the UV to the NIR.

Resumen

Los láseres con realimentación distribuida (DFB) son unos de los láseres de película delgada más estudiados ya que son económicos, compactos y puedes ser fácilmente integrados en otros dispositivos. Además, son útiles para un gran número de aplicaciones, como espectroscopía, comunicaciones ópticas o sensores. Un láser orgánico DFB consiste en una capa activa orgánica depositada sobre una red de difracción grabada en un sustrato inorgánico (configuración estándar), pero puede presentar distintas arquitecturas dependiendo de la posición de la red y de los materiales con los que esté fabricada. En este trabajo se estudia una arquitectura láser DFB con un resonador polimérico depositado sobre la capa activa. Esta arquitectura ofrece ciertas ventajas frente a las configuraciones más habituales. Este tipo de dispositivos son sencillos de fabricar, ya que las dos capas se pueden preparar a través de disolución, su capa activa presenta un espesor uniforme y el periodo de la red de difracción se puede ajustar fácilmente para cada caso debido a su fabricación mediante litografía holográfica.

En esta tesis, la optimización de los láseres DFB se ha logrado mediante dos vías distintas: mediante la optimización del resonador mediante el control de sus parámetros geométricos y de fabricación y mediante el diseño y fabricación de láseres DFB optimizados para nuevas moléculas orgánicas que se han utilizado como material activo. El primer paso en la optimización del resonador fue un estudio sistemático del efecto de los parámetros de fabricación en las características de emisión finales de los dispositivos. Después, se analizó la capacidad del material de fabricación de las redes (gelatina dicromatada, DCG) para ser utilizado en láseres que emiten en la parte baja del espectro visible. Por último, se comparó la arquitectura con el resonador sobre la capa activa frente a la configuración estándar bajo variables no consideradas anteriormente para comprobar la mejora de su rendimiento, como el uso de un material activo en altas concentraciones que modifica el índice de refracción de la capa activa. Además, el proceso de fabricación fue mejorado mediante el estudio e implementación de un nuevo método espectrofotométrico para medir el espesor y el índice de refracción de capas delgadas poliméricas, que conllevó una optimización de los dispositivos fabricador. Una vez optimizado el resonador, se fabricaron láseres DFB y se adaptaron a diferentes materiales activos. Se estudiaron diversas familias de nuevos compuestos, con emisiones desde el ultravioleta hasta el infrarrojo cercano.

List of Figures

List of Abbreviations

ASE Amplified spontaneous emission

COPV Carbon-bridged oligo(p-phenylenevinylene)

DCG Dichromated Gelatine

DFB Distributed Feedback

HL Holographic Lithography

LSE Laser Slope Efficiency

OP Optical Polymer

OSC Organic Semiconductors

PAH Polycyclic Aromatic Hydrocarbon

PL Photoluminescence

PLQY Photoluminescence Quantum Yield

PS Polystyrene

TFOL Thin Film Organic Laser

Contents

Contents

Part I

Introduction

1 Photophysics fundamentals

1.1 Laser

Lasers are one of the most important technologies developed in the 20th century, along with the transistor and the computer [1] and the word laser is an acronym for Light Amplification by Stimulated Emission of Radiation. Its main physical principle is the stimulated emission, proposed by Einstein in 1917 [2], which led to the understanding that the incident and the emitted photons from excited atoms are identical [3]. The first theoretical approach to the concept of laser was suggested in 1940 by Fabrikant [4] and was further explored by Townes et al. with the fabrication of the maser in 1958, which operated in the microwave range [5]. The first laser was fabricated by Maiman in 1960 using a rod of synthetic ruby crystal with reflecting coatings [6] and in 1964 the Nobel Prize in Physics was awarded to Charles Townes, Nicolay Basov, and Aleksandr Prokhorov "for fundamental work in the field of quantum electronics, which has led to the construction of oscillators and amplifiers based on the maser-laser principle" [1,7]. So many other Nobel prizes involving the laser advances have been awarded, such as the 1966 award to Albert Kastler for his work on optical pumping techniques or the 1981 prize to Bloembergen and Schawlow for laser applications in spectroscopy [7].

Lasers present four key elements: gain medium, pumping process, optical cavity or resonator and output light [8,9]. The gain or active medium is the collection of atoms or other materials that amplify the light signal directed to it by stimulated emission. This stimulation is produced by the pumping process, which excites the active material into higher energy levels. Then, the optical cavity holds the amplified light and redirects it through the gain medium repeatedly to improve the amplification. Lastly, part of the light stored in the cavity is extracted from it to be used in the desired application. This tends to be the secondary function of the optical cavity, such as a mirror without perfect reflectivity (see Figure 1.1).
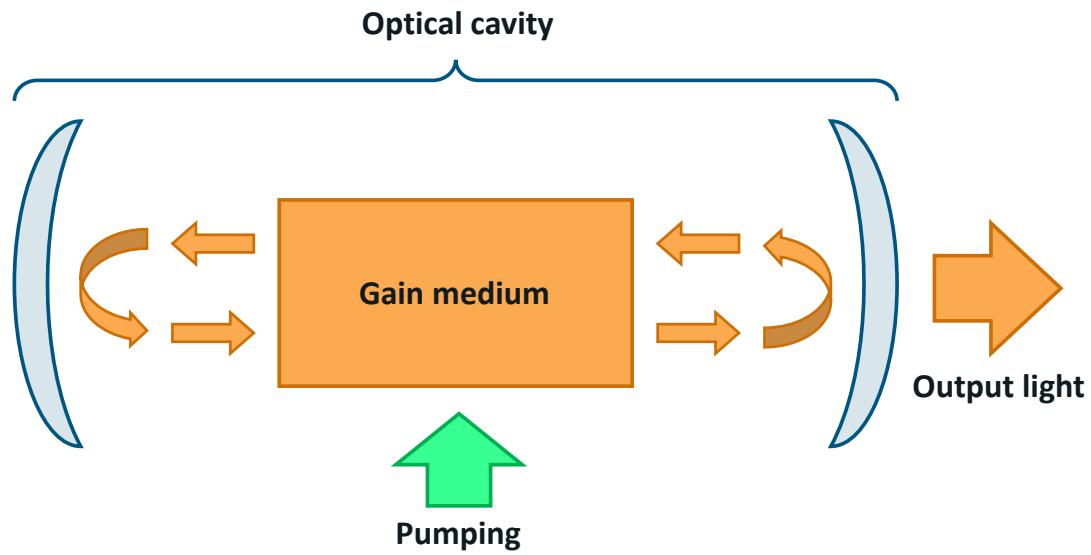
Figure 1.1: Scheme of the basic elements of a laser

1.1.1   Light matter interactions

The interaction between light and matter can take place by three different processes [10]:

- **Absorption**: the energy of an incident photon is transferred to an electron as potential energy when it changes from state E_m to E_n. The absorption probability of an electron is B_{mn}.

- **Spontaneous Emission**: when an electron in an atom is in an excited state E_n, it has a probability A_{nm} to spontaneously decay to the lower state E_m. The energy of the emitted photon will be $E_n - Em = h\nu$ and its direction, phase and polarization will be random quantities

- **Stimulated Emission**: only occurs under the influence of an electromagnetic wave. If a photon with energy $h\nu$ passes by an excited atom, it can stimulate the emission by this atom. The probability of this process is B_{nm}, which is equal to the absorption probability B_{mn}. The emitted photon will have the same energy, direction, phase and polarization as the original photon.

1.2   Light amplification

The stimulated emission can be used to amplify electromagnetic waves under certain conditions [10]. Let's consider a material with two energy levels E_1 and E_2 an N atoms.

Each level is populated with N_1 and N_2 atoms per unit level respectively. If the system is illuminated by a beam of n photons per second per unit volume with an energy of $h\nu = E_2 - E_1$, the absorption probability will be proportional to the number of photons in a position z in the medium and to the population of atoms in the level E_1. Then the variation of photons n in terms of the distance z inside the material will follow:

$$\frac{\mathrm{d}n}{\mathrm{d}z} = (N_2 - N_1)b_{12}n + a_{21}N_2 \tag{1.1}$$

where $b_{12} = b_{21}$ and a_{12} are proportional to the Einstein coefficients. Assuming the spontaneous emission is of no importance in this process, the number of photons through the propagation distance is

$$n(z) = n_0 \, \mathrm{e}^{(N_2 - N_1)b_{12}z} \tag{1.2}$$

being n_0 the number of incident photons.

Then, we can distinguish three cases depending on the populations N_1 and N_2. If $N_2 < N_1$, we have the situation of any absorbing material at room temperature, with more atoms in the ground state than in the excited state. The equation 1.2 will then be reduced to the Beer-Lambert law for absorption with $(N_1 - N_2)\,b_{12} > 0$ being the absorption coefficient. If $N_1 = N_2$, the number of photons is constant for all the propagation distance. As the absorption and stimulated emission coefficients are the same, these two process will be balanced. If we consider the effect of the spontaneous emission in equation 1.2, the number of photons will slightly increase with distance. When $N_2 > N_1$, there are more atoms in the excited state than in the ground one and the population is "inverted". Equation 1.2 can be written as $n(z) = n_0 \mathrm{e}^{gz}$, where $g = (N_1 - N_2)b_{12}$ is the gain coefficient. This produces a chain reaction, as every photon stimulates the emission of a twin photon which will again induce the emission of another photon. However, this does not mean that the photons are doubling in every generation, as we also must take into account that the emitted photons are resonant with the two-level system and some of them will be reabsorbed, while some of the excited atoms will present a spontaneous decay. To consider every loss channel, it is useful to define a net optical gain for real systems given by [3]:

$$g' = g - \alpha \tag{1.3}$$

which gets positive values when the threshold for amplifying radiation has been reached. It is important to notice that the inverted population needed to obtain gain and light amplification is not possible in a two-level system. The stimulated emission from the atoms in the excited states makes them go back to the fundamental level, so the absorption and stimulated emission would eventually compensate and reach an equilibrium. This problem is solved with the consideration of three-level and four-

level systems. Those two system can be used to get an inverted population, but the four-level one is more efficient and is the preferred one used to model laser media [11].

Light amplification in a material can be produced by three different processes: superradiance, superfluorescence and amplified spontaneous emission (ASE). Both superradiance and superfluorescence are characterized by a threshold as they are cooperative spontaneous emission processes from a set of dipoles. However, ASE is a collective effect, as the light amplification is produced as the spontaneous emission provokes further emission in materials with a high optical gain. The effect of the ASE is an increase radiation emitted along the axis of the active material without any resonant cavity. It is very dependent on the geometry of the active medium, typically with one dimension significantly larger than the others, and the effect in the emission spectra is a narrowing of the photoluminescence (PL) around the maximum gain wavelength.

Even if ASE process does not have inherently a threshold, it is common to define it as the pump energy at which the emission linewidth starts to decrease [12]. It is useful to compare the optical gain of different materials when prepared with the same geometry and to check their capacity to be used as active material for lasing devices.

1.3 Waveguides theory

One of the most useful configurations to explore the optical gain of a material is the optical waveguide [13]. There are different kind of waveguides with different dimensions of confinement, but we are going to focus on planar with a step-profile refractive index, which are the most commonly used for this purpose due to its simple fabrication process. We assume the waveguide's refractive index (n_f) is higher than the one of the substrate (n_s) and the cover (n_c). In addition, we can also consider the typical situation where $n_s > n_c$.

Let us first consider the analysis using ray optics and then we will complete the results analyzing them with an electromagnetic wave treatment. The critical angles in the cover-film (θ_{1c}) and in the film-substrate interface (θ_{1c}) are [13]:

$$
\begin{aligned}
\theta_{1c} &= \sin^{-1}\left(n_c/n_f\right) \\
\theta_{2c} &= \sin^{-1}\left(n_s/n_f\right)
\end{aligned}
\tag{1.4}
$$

Given the previous conditions, we have that $\theta_{2c} < \theta_{1c}$. Depending on the value of the propagating angle in the film, θ, we can have 3 different cases:

- $\theta < \theta_{1c}$: the light will penetrate both the cover and the substrate, so the radiation is not confined to the film.

- $\theta_{1c} < \theta < \theta_{2c}$: the light will penetrate the substrate but will be totally reflected by the cover.

- $\theta_{2c} < \theta < 2\pi$: corresponds to a guided mode, as the ray can not penetrate neither the substrate nor the cover, so it will be total confined in the film..

In a roundtrip inside the film, the phase shift of the ray changes due to the film thickness and to the reflection at the two boundaries. This shift is given by:

$$\phi = 2k_x \, d = 2k_0 \, n_f \, d \cos \theta \tag{1.5}$$

where $k_0 = \pi \lambda^{-1}$ is the wavevector and k_x its x-component. Considering ϕ_c and ϕ_s the phase shifts produced in the interfaces, we have:

$$2k_0 \, n_f \, d \cos \theta - \phi_c - \phi_s = 2\pi m \tag{1.6}$$

with m as the mode order. This is a transcendental equation that can be solved numerically for a particular mode order to obtain the mode propagation angle θ_m. Based on this angle we can define the propagation constant β_m, which links the geometrical explanation of the phenomena (angle θ_m) with the electromagnetic treatment:

$$\beta_m = k_0 \, n_f \sin \theta_m = k_0 \, n_{eff} \tag{1.7}$$

where n_{eff} is the effective refractive index and acts as a weighted average refractive index of the mode propagating through the waveguide.

To analyze the problem from the electromagnetic point of view, we will obtain the wave equations for TE and TM modes in planar waveguide when every layer has a constant refractive index. If the light propagating media are dielectric (conductivity $\sigma = 0$), non-magnetic (magnetic permeability $\mu = 0$), isotropic and linear, Maxwell equations can be written as [13]:

$$\nabla \times \vec{E} = -\mu_0 \frac{\partial \vec{H}}{\partial t}$$
$$\nabla \times \vec{H} = -\epsilon_0 \, n^2 \frac{\partial \vec{E}}{\partial t} \tag{1.8}$$

Where $\vec{E}$ is the electric field, $\vec{H}$ the magnetic field, ϵ_0 the permittivity, μ_0 the permeability and n the refractive index of the propagating medium. If this medium is optically inhomogeneous, the refractive index depends on the position and the Maxwell equations can be derived as:

$$\nabla^2 \vec{E} + \nabla \left(\frac{1}{n^2} \nabla n^2 \vec{E} \right) - \epsilon_0 \, \mu_0 \, n^2 \frac{\partial^2 \vec{E}}{\partial t^2} = 0$$
$$\nabla^2 \vec{H} + \frac{1}{n^2} \nabla n^2 \times (\nabla \times \vec{H}) - \epsilon_0 \, \mu_0 \, n^2 \frac{\partial^2 \vec{H}}{\partial t^2} = 0 \tag{1.9}$$

7

For planar waveguides, the refractive index only depends on one coordinate, $n = n(x)$, and setting the propagation direction as the z-axis, we obtain the following solution for the electric and magnetic fields [13]:

$$
\begin{aligned}
\vec{E}(\vec{r}, t) &= \vec{E}(x) \, \mathrm{e}^{i(\omega t - \beta z)} \\
\vec{H}(\vec{r}, t) &= \vec{H}(x) \, \mathrm{e}^{i(\omega t - \beta z)}
\end{aligned}
\tag{1.10}
$$

This will provide the solutions for the electric and magnetic fields for the different operating modes in the waveguide. As stated before, this solution incorporates the propagation constant β_m, which can also be related to the geometrical parameters θ_m and n_{eff}. This n_{eff} of a certain guided mode increases with the thickness variation. That means, that for a certain thickness, not every TE and TM mode will be able to exist in the waveguide. The minimal thickness that allows a certain mode to be guided is the cut-off thickness $h_{\text{cut-off}}$, and can be calculated from their dispersion equations [14]:

$$
h_{\text{cut-off}} \, (\text{TE}) = \frac{m\pi + \arctan \sqrt{\dfrac{n_s{}^2 - n_c{}^2}{n_f{}^2 - n_s{}^2}}}{k \sqrt{n_f{}^2 - n_s{}^2}}
$$

$$
h_{\text{cut-off}} \, (\text{TM}) = \frac{m\pi + \arctan \left[\left(\dfrac{n_f}{n_c} \right)^2 \sqrt{\dfrac{n_s{}^2 - n_c{}^2}{n_f{}^2 - n_s{}^2}} \right]}{k \sqrt{n_f{}^2 - n_s{}^2}}
$$

$$
\tag{1.11}
$$

1.4 Distributed feedback lasers

The optical cavity of a laser can present different configurations [15–18]. We are going to focus in one kind that is really suited to work with the previously studied waveguide structures, the distributed feedback (DFB) laser. This was proposed by Kogelnik and Shank in 1972 [19] and consists of a periodic modulation along a waveguide of the refractive index or of the gain. The modulation provides feedback in the waveguide structure and, therefore, laser emission whose wavelength can be easily tuned.

The basic condition to obtain DFB is the conservation of the optical wavevector in one dimension. Considering a periodical waveguide with a grating period Λ, a reciprocal lattice vector k_g and an optical wave with a wavevector $+\beta$, we have that:

$$
\begin{aligned}
|\vec{k_g}| &= \frac{2\pi}{\Lambda} \\
|\vec{\beta}| &= \frac{2\pi n_{eff}}{\lambda}
\end{aligned}
\tag{1.12}
$$

The grating scatters the wave into a counter propagation wavector $-\beta$ and the momentum is conserved, so we obtain

$$\vec{\beta} - m\vec{k_g} = -\vec{\beta} \tag{1.13}$$

which leads to the Bragg condition for the DFB

$$m\,\lambda_B = 2\,n_{eff}\Lambda \tag{1.14}$$

In the case of second order (see figure 1.2), the first order scatter will be present resulting in a zero in-plane wavevector, and the energy conservation will be achieved with the radiation of a wave perpendicular to the surface.

(a)   (b)
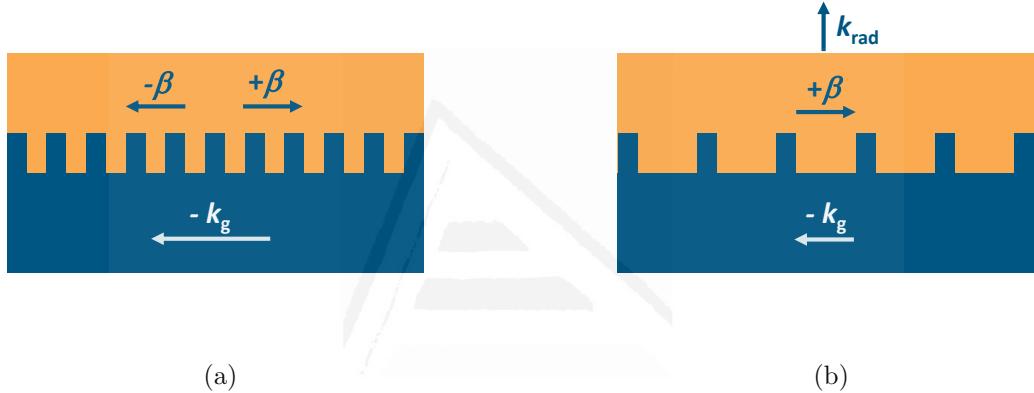
Figure 1.2: (a) Feedback in a first-order DFB grating (b) Radiating wave in a second-order DFB grating. Provisional image from [3], to be changed.

According to Kogelnik and Shank [19], the electric field in the DFB lasers can be modeled using the coupled mode theory with the scalar Helmholtz wave equation.

$$\left[\nabla^2 + k^2\right] E(x,z) = 0 \tag{1.15}$$

For the second order DFB, the electric field test in the scalar Helmholtz equation is [3]:

$$E(x,z) = \left[A(z)\mathrm{e}^{i\beta_0 z} + B(z)\mathrm{e}^{-i\beta_0 z}\right]\phi(x) + \Delta E(x,z) \tag{1.16}$$

where $A(z)\mathrm{e}^{i\beta_0 z}$ and $B(z)\mathrm{e}^{-i\beta_0 z}$ being the amplitude of two propagating waves along the z axis, $\phi(x)$ the transverse mode profile and $\Delta E(x,z)$ represents the perpendicular radiated wave. The presence of gain or refractive index modulation introduces a perturbation to the Helmholtz equation [3]:

$$k_z{}^2 = \beta^2 + 2i\beta g_\omega - \frac{\omega^2}{c^2}\Delta\epsilon \sum_{m\neq0}\int \xi_m(x)\,\phi(x)\,\mathrm{d}x\,\mathrm{e}^{2m\,i\beta_0 z} \tag{1.17}$$

9

where g_ω is the net gain at a given frequency, $\Delta\epsilon$ the difference in dielectric constant throughout the modulated interface and $\sum_{m\neq 0} \int \xi_m(x)\,\phi(x)\,d\,x\,\mathrm{e}^{2m\,i\beta_0 z}$ a Fourier series for the periodic structure.

The final solutions for the second order DFB coefficients A (z) and B(z) are [3]:

$$A(z) = \sinh\gamma z$$
$$B(z) = \pm\sinh\gamma(z-L) \tag{1.18}$$

with L being the DFB structure length and the complex propagation constant defined as

$$\gamma^2 = (g_\omega - i\Delta\beta - \kappa_r)^2 - (i\,\kappa_f - \kappa_r)^2 \tag{1.19}$$

Finally, the feedback and radiative coupling coefficients, κ_f and κ_r, can be expressed as [3]:

$$\kappa_f = \frac{-\,\omega^2\Delta\epsilon}{2\,\beta_0\,c^2}\int \mathrm{d}x\,\phi(x)^2\,\xi_2(x)$$

$$\kappa_r = \frac{\omega^4\Delta\epsilon}{4\,\beta_0\,\beta_x\,c^4}\left|\int \mathrm{d}x\,\mathrm{e}^{i\beta_x x}\,\phi(x)^2\,\xi_1(x)\right|^2 \tag{1.20}$$

In the second order DFB, the second-order Fourier coefficient (ξ_2) is the one responsible for the feedback, while the first-order coefficient (ξ_1) acts as a loss mechanism as it indicates the strength of the radiated wave.

2 State of the art

Organic materials have received great attention in the last years since they are cost-effective, easy to manufacture and their optoelectronic properties can be tuned through molecular design [15, 16]. These characteristics makes them capable to be used in a wide range of optoelectronic applications, such as light-emitting diodes, solar cells, transistors or lasers [20]. In particular, laser development adopted the use of organic systems as active materials since the very beginning of its existence, as the first two organic lasers [21, 22] were developed in 1966, just six years after the presentation of the first laser by T. Maiman [6].

Since then, organic materials have been developed to improve their performance in organic lasers. The advances in chemical design allowed to perform modifications of previous materials and the synthesis of new ones in order to obtain the desired functionalities. These efforts were mainly directed to reduce the pump intensity needed for their operation (the threshold), improve the photodegradation, allow emission in the whole visible spectrum, improve their processing versatility and facilitate the integration of the resulting lasers with other devices [3]. All these improvements made possible the realization of low-cost, flexible and integrated lasers, reaching milestones such as the first LED pumped organic laser [23], the observation of lasing behaviour in a living system [24] or the first electrically pumped organic laser [25].

2.1 Organic active materials

The development of organic active materials has been prolific throughout the years. This has resulted in a wide variety of materials that can be divided in two main groups: dyes and organic semiconductors (OSC) [3, 16]. Organic dyes are π-conjugated molecules with a high fluorescence quantum yield. They are typically good emitters in a diluted form (in a solvent or solid matrix), but fluorescence quenching generally appears when their doping rate into the matrix is high due to the interaction between nearby molecules. The first dye organic lasers were prepared in liquid solutions, but for the preparation of solid state lasers, solid hosting materials were used. Among them, thermoplastic polymers, such as PS or PMMA [26] are very common and ideal for thin-fim (waveguide-based) devices. OSCs, on the other hand, are characterized for their

charge transport and electroluminescence properties [27], and can be divided into the following categories: organic crystals, small molecules, dendritic starburst molecules and conjugated polymers [20]. Nevertheless, the charge transporting property is not normally used because devices are pumped optically (except for few exceptions). Lasers based on conjugated polymers generally show lower thresholds than those based on dye-doped systems because they can be prepared as neat (undiluted) films. On the other hand, their photostability is generally lower.

In this thesis we have focused on solid state lasers with organic molecules dispersed in polymeric matrices as active media. More specifically, on thin-film organic lasers (TFOLs) in which the films constitute waveguides. The particular compounds used belong to two families of materials with great potential to be used in this kind of application: Carbon-bridged oligo(p-phenylenevinylene)s (COPVs) and polycyclic aromatic hydrocarbons (PAHs).

2.1.1 Carbon-bridged oligo(p-phenylenevinylene)s (COPVs)

Materials based on phenylenevinylene (PV) are some of the most investigated in the organic electronics field. Poly(phenylenevinylenes) (PPVs) such as MEH-PPV were the first examples of organic semiconductors lasers [28, 29]. Other PV polymers and oligomers (OPV) have also been used for diverse optoelectronic applications [18, 30]. Recently, some new OPV derivatives have shown excellent lasing properties: the carbon-bridged oligo(p-phenylenevinylene)s (COPVn, with n= 1 to 6) [31]. These oligomers were prepared by the insertion of carbon bridges between the phenylene and vinylene units, which resulted in planar oligomers that presented high photoluminescence quantum yield (PLQY) values. Besides, they were more stable than conventional OPVs due to the protection of the middle part of the molecule [32–34]. COPVn based lasers present one key characteristic that makes them suitable for diverse applications: the possibility of tunning the emission wavelength by changing the length of the oligomer. The longest COPVn compounds ($n > 3$) presented an excellent performance in terms of threshold and photostability, while the shorter compounds, whose emission is in the blue, had a more limited performance due to the reactive terminal sites in the photoexcited states [35].

2.1.2 Polycyclic aromatic hydrocarbons (PAHs)

Since the isolation of graphene in 2004 by Novoselov et al. [36], the interest in polycyclic aromatic hydrocarbons (PAHs) increased drastically. These nanoscale graphenes include variations such as graphene nanoribbons and graphene quantum dots, and are suitable semiconductors for electronic applications as they present finite band gaps due to the quantum confinement [37].

In particular, large-size disk-like PAHs present strong intermolecular $\pi - \pi$ stacking along their columnar superstructures, which makes them suitable for charge transporting, but the aggregation limits their light emitting properties, as it quenches the photoluminescence [38–40]. Some strategies to avoid this effect involves the attachment of long branched alkyl or alkylphenyl chains in order to increase their solubility and avoid the molecular interactions [41], but it tends to not be enough to avoid PL quenching. Another possible strategy to improve the PLQY of these materials is focused on their edge structure, as different end topologies (armchair, zigzag, cove...) affect significatively to their optical properties [42, 43].

These strategies to obtain light emitting PAH have already been used. The first nanographenes with ASE emission were presented by Paternò et al. in 2017 [44] and the first laser using nanographenes as active materials are presented in this thesis (Publication 6). Our research group, along with our collaborators, has focused on laser fabrication using these kind of materials, such as publication 7 that presents lasers with PAH as active materials and some other publications that are not included in this thesis [45–48].

2.2 Laser resonators

In the development of the laser technology, the other important aspect besides the study of the active materials is the optical cavity or resonator. In this section, we are going to explore the most widely used resonators in TFOLs and their differences. Even if the use of an organic gain medium is enough to consider a laser as organic, there are some of the optical cavities which also include organic materials as resonators, achieving all-organic laser devices.

The first and most direct form organic lasers are planar cavities, with two mirrors enclosing a planar organic cavity, forming a Fabry-Perot optical microcavity (feedback occurs in a direction perpendicular to the film plane) [16]. Their structure resembles the one from the stacked OLEDs, so this can be an advantage as they can benefit from the developments on that other field. The mirrors can be evaporated metal surfaces or distributed Bragg reflectors (DBR), which achieve lower thresholds due to their higher reflectance [18].

Some other microcavities with different geometries are often used as organic lasers, taking advantage of the good processability of the organic materials. For example, microrings can be obtained by dipping a fiber of the active material into solution with a polymer. The light can travel through the formed microring using internal reflections, combining the waveguide modes and the whispering gallery modes. Similarly, microdisks can be easily fabricated with lithography etching. The light in these microdisks also supports whispering gallery modes, along with Fabry-Perot resonances. And finally, microspheres can be formed as the junction of several microdisks. Micro-

cavities generally present good performance, but the output light is emitted in many radial directions, difficulting the integration of these resonators in photonic circuits [18].

One of the most widely used TFOLs is the distributed feedback (DFB) laser. Its physics fundamentals were explained in section 1.4. The DFB laser consists on a planar waveguide which includes a modulation in its refractive index or gain. The most common organic DFB is based on an active film deposited over a periodic corrugated substrate, which provides the feedback and amplification of the emitted light. The direction of the output light depends on the diffraction mode used by the DFB, being in the direction of the waveguide for $m = 1$ and perpendicular to the surface for $m = 2$. This facilitates the integration of these kind of lasers in different optical devices [16].

2.2.1 Types of DFB resonators

Distributed feedback lasers can present different architectures, depending on the placement of the periodic corrugation and the material [49]. As stated before, the standard configuration consist of an inorganic substrate with a corrugation etched on its surface, and an active layer deposited on top of it. Devices with this configuration have generally reached the lowest threshold values [50], but an important drawback is that they are not all-organic devices. This makes processing more difficult and limits their integration with other devices. As an alternative, the corrugation can be directly engraved on top of the active film [51]. This facilitates the fabrication process, but the quality of the waveguide or the optical properties of the active film can be affected negatively affected by the processes used to engrave the grating. For example, the high pressure and temperature used in nanoimprint lithography.

Another alternative, which is the one followed in this thesis, implies the use of an additional polymeric film in which the corrugation is engraved. We differentiate two cases: with this resonator layer located below the active film (between the substrate and the active film, RB configuration); or with the resonator on top of the active film (RT configuration). The RB configuration is similar in geometry to the standard configuration, but in this case the grating is made of organic material. Note, however, that the refractive index contrast between the grating and the active layer is lower than in the standard case [49], which contributes to a higher threshold in this configuration. On the other hand,for RT configuration the refractive index contrast improves is not between two organic materials, but between the grating and the air, which leads to an improvement in the contrast and therefore the lasing threshold. Additionally, this configuration has the advantage of preserving the active layer completely planar, which also contributes to an optimization of the device and a lower threshold [49].

3 Main results

3.1 Objectives

The objective of this work is the optimization of DFB lasers based on polymeric diffractive resonators prepared as separated layer located on top of the active films (the so-called top-layer resonator architecture). This is divided in two main objectives:

a) Resonator optimization, through a fine control of fabrication and geometrical parameters, to improve DFB laser performance

b) Design and fabrication of optimized DFB lasers for new organic molecules to be used as active materials

Firstly, to optimize the devices performance, a systematic study of the influence of several parameters of the grating fabrication process (initial layer thickness, exposure time, development time...) on the grating final characteristics was performed, analyzing the influence of these parameters on the emission properties of the final DFB lasers with the grating on top of the active film. Additionally, the capacity of the material used for the grating fabrication (dichromated gelatin, DCG) to fabricate DFB lasers emitting at a lower wavelengths was studied. The DFB laser architecture used was compared to the standard one under new variables to check its improved performance.

After this optimization was performed, adequate gratings and DFB devices were able to be fabricated adapted to different active materials. Various families of compounds, whose synthesis constituted a major contribution in the Chemical context, with emissions ranging from the UV to the NIR, have been studied.

3.2 Published papers

The results of this thesis are presented as a compendium of the following publications, which can be found in part II:

Publication 1. Controlling the emission properties of solution-processed organic distributed feedback lasers through resonator design

Publication 2. Blue and deep-blue-emitting organic lasers with top-layer distributed feedback resonators

Publication 3. N,N'-Bis(3-methylphenyl)-N,N'-dyphenylbenzidine based distributed feedback lasers with holographically fabricated polymeric resonators

Publication 4. Sub-400 nm film thickness determination from transmission spectra in organic distributed feedback lasers fabrication

Publication 5. Simultaneous determination of refractive index and thickness of submicron optical polymer films from transmission spectra

Publication 6. Solution-processed nanographene distributed feedback lasers

Publication 7. Perylene-fused, aggregation-free polycyclic aromatic hydrocarbons for solution-processed distributed feedback lasers

Publication 8. Kinetically protected carbon-bridged oligo(p-phenylenevinylene) derivatives for blue color amplified spontaneous emission

3.3 Results

This section contains the main results obtained throughout the thesis, which will be fully developed in chapter II in the different publications that conform this thesis.

As it has been stated in section 3.1, the first objective of this thesis is the optimization of DFB laser devices with the resonator on top of the active film. In order to do that, the influence of the resonator geometry on the emission properties of these devices was studied in publication 1. On DFB lasers with this architecture, the active layer presents a uniform thickness as the resonator grating is an independent layer. This disposition has some advantages in terms of the laser threshold and the laser slope efficiency (LSE), but additionally it allows modifying the emission properties by changing the geometric parameters of the resonator, without any modification of the active layer. In our case, we focused our attention on two parameters: the residual layer thickness (the layer separating the active film and the grating) and the grating depth.

Furthermore, the grating fabrication process was made using a novel dry-development process, consisting of an oxygen plasma produced by a simple plasma cleaner machine.

This, along with the fact that both, the active layer and the resonator are solution-processed, provides an overall simple, cost- effective and scalable device fabrication process.

The lasing threshold and the LSE are analyzed in Figure 3.1 in terms of the residual layer thickness and the grating depth. The curves shown correspond to different initial thickness of the DCG layer. For every curve, as the development time increases, so does the grating depth while the residual layer decreases, up to a point when there is no residual layer (dashed line). The results show that the lesser the residual layer, the better the overall performance of the device, as the lasing thresholds decreases while the LSE increases. The effect of the grating depth is not so simple to analyse, as both the lasing threshold and the LSE increase with the grating depth, so it will be necessary to reach a compromise between both parameters. As it can be observed in Figure 3.1b, the LSE increase with the increase of grating depth; but it gets to a limit because the grating is less efficient as its depth gets bigger as most of the light is confined in the active layer. Taking this into account, the optimal value of the grating depth is set in the 100-130 nm range, which has an optimized lasing threshold of around 25 μJ/cm^2 and a LSE of about 80% of the maximum attainable value.
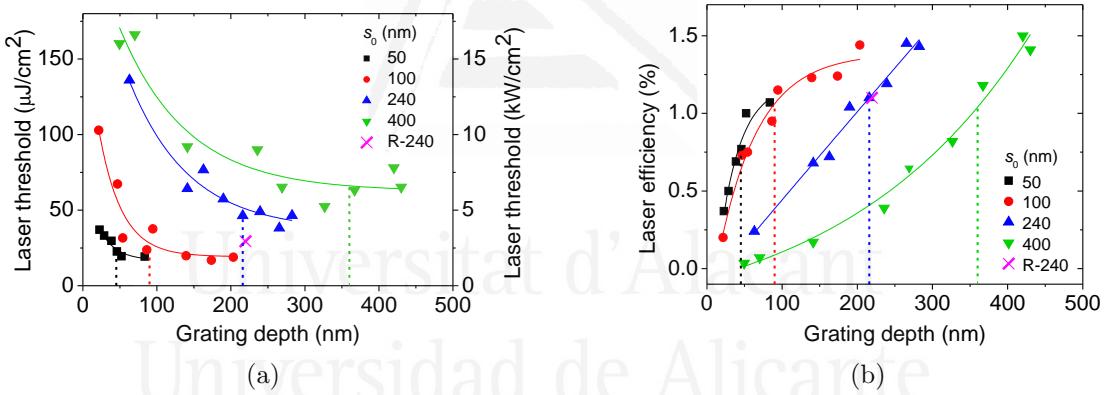

Figure 3.1: Laser threshold (a) and laser efficiency (b) as a function of the grating depth for different initial values of initial resist layer thickness, s_0 (see legend).

The next step was to study the possibility of the DCG gratings to act as resonators in deep-blue-emitting DFB lasers. Up to this moment, DFB devices with this architecture had been made using active materials emitting in the green and red windows of the visible spectrum. To test the viability of the DCG gratings in this application, several of them with different periods were fabricated by HL and it was checked that the grating resolution was maintained throughout the whole range studied, as they all have the same grating depth (see Figure 3.2a).

Additionally, the grating profile of the square gratings used was analysed through simulation of the coupling coefficients (both κ_1, which describes the losses, and κ_2, which refers to the feedback) as a function of their duty cycle. The results are shown in Figure 3.2b for two different gratings with periods corresponding to devices with

COPV1(Me)-*t*-Bu and COPV2-Tip as active materials, emitting at 376 nm and 474 nm respectively. The duty cycles used in our devices is around 0.75 and in Figure 3.2b can be checked that this value maximizes the feedback while reducing the losses at the same time, so it is a great choice to optimize the device performance.

Finally, DFB devices with top resonators emitting in the deep-blue and blue window of the visible spectrum were fabricated. Different materials were used, thanks to the collaboration of Dr. Naiti Lin and Prof. Eiichi Nakamura (from the University of Tokyo), Shoya Watanabe and Prof. Hayato Tsuji (from Kanagawa University), and Dr. Karolis Kazlauskas, Dr. Ona Adomeniene and Prof. Saulius Jursenas (from Vilnius University) who provided the active materials. Among all these materials, COPV1(Me)-*t*-Bu (provided by the groups of Prof. Eiichi Nakamura and Prof. Hayato Tsuji) was the one with the lowest emission wavelength and its chemical synthesis and complete optical characterization was also included in the publication. We were able to fabricate DFB lasers for every material, improving the threshold value for the materials previously reported [31] and getting wavelength tunability for all of them thanks to the versatility offered by HL to easily fabricate gratings with different periods. The successful application of this DFB architecture to materials emitting in the deep-blue range has expanded its utilization with a wide range of materials for different applications.
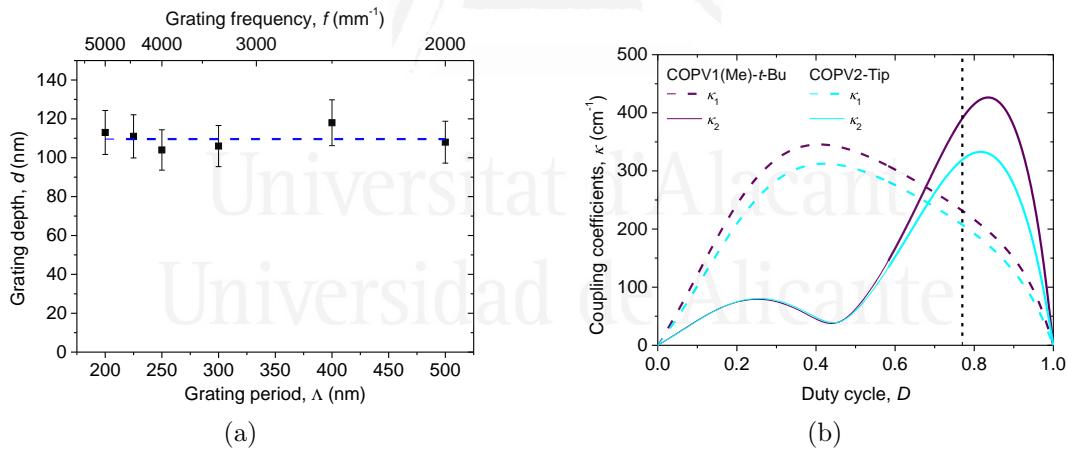
Figure 3.2: (a) Grating depth evolution with the grating period to evaluate the resonator resolution of the fabrication process; (b) Effect of the duty cycle, D, on the coupling coefficients for 2nd order DFB lasers with top-layer resonator.

After analyzing the capabilities of the top layer resonator DFB devices (RT architecture), we performed a detailed comparison with devices in which the resonator is located below the active layer (RB architecture) (Publication 3). The RB configuration is similar to the standard one typically used in this kind of lasers, although in that case the grating is engraved in an inorganic substrate [49]. The active material used in this comparison was N,N'-bis(3-methylphenyl)-N,N'-dyphenylbenzidine, also known as TPD. This material has mainly been used in optoelectronic applications as

a hole-transport material and its emitting properties have not been widely exploited.

An important feature of TPD is that it can be dispersed in the polymeric hosting matrix (typically polystyrene) at large doping rates without PL concentration quenching effects. In fact, TPD shows ASE as a neat film (without dispersion in a matrix) [52]. This allows a proper comparison between the two configurations taking into account parameters that could not considered when the RT configuration was used with other dyes. In those cases, the maximum dye concentration in the active film used was 5 wt%. Consequently, the refractive index of the active film was that of the inert polymer acting as a matrix and the contrast between the active film and the grating in the configuration RB was quite low. TPD active films can vary their concentration in the inert polymer matrix and therefore their refractive index, which leads to a better contrast between this layer and the resonator and to a better confinement of the guided mode in the waveguide, increasing the efficiency of the RB configuration.

DFB laser devices with different TPD concentrations ranging from 5 wt% to 60 wt% in a PS matrix were fabricated using the two configurations, RB and RT. The influence of the concentration in the lasing threshold and in the photostability is presented in Figure 3.3. For concentrations higher than 20 wt%, both configurations present a constant lasing threshold of around 180 μJ/cm^2. The treshold increases for lower concentrations as the material absorption also decreases and is less efficient. However, there are significant differences between the two configurations, being the RT configuration the one which preserves a lower threshold in this range of concentrations. This can be explained in terms of the mode confinement in the waveguide, which is higher for the RT configuration for each TPD concentration.
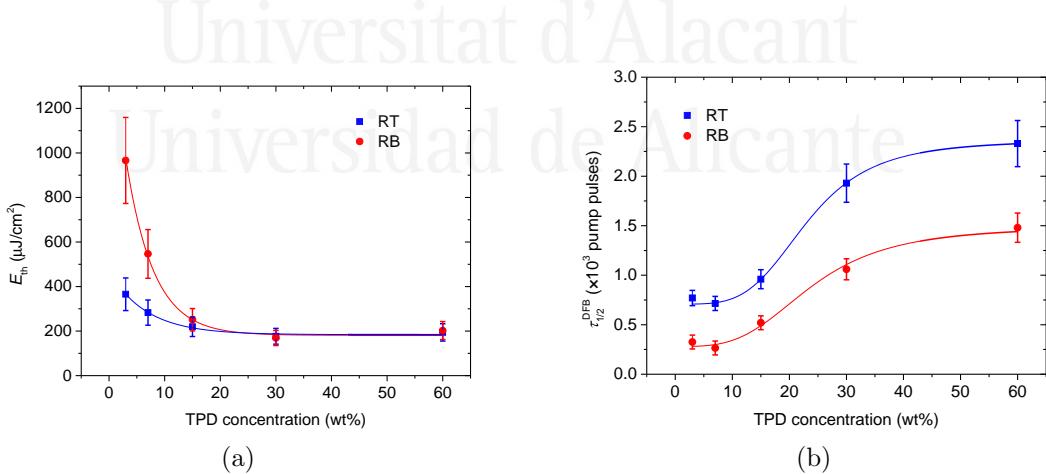
Figure 3.3: (a) Laser threshold and (b) Photostability of DFB lasers with different TPD concentrations for RB and RT configurations

Lastly, the photostability is better for the RT configuration for every concentration, approximately twice higher. The main reason is the protecting effect of the DCG layer when it is placed on top of the active film doped with TPD, as it prevents its photooxidation under UV light exposition. Taking all this into account, DFB devices

with the RT configuration show an overall better performance, in terms of both, the lasing threshold and the photostability, than the ones with RB configuration.

In the field of TFOLs, it is important to have a good control of the device fabrication parameters, such as the thickness of the different films included in the device, so the performance can be optimized and is reproducible. Most of the commonly used methods to measure film thickness are destructive, such as scanning electron microscopy (SEM), atomic force microscopy (AFM) or profilometry. In our case, we considered the use of non-destructing methods to be vital, as this allows the control of the fabrication process and the optimization of the devices that will actually be used. The two most common non-destructive methods are the ellipsometry and the spectrophotometric methods. The former presents great sensitivity, even for films of a few nanometers. The spectrophotometric methods are less precise and are limited to thicker films, but in return they are cost-effective, with a simpler analysis and require less time.

A common spectrophotometric method to measure film thickness is the envelope method, proposed by Manifacier in 1976 [53] and also known as Swanepoel envelope method, as he further developed and popularized it [54, 55]. This method is based on the analysis of the interference pattern present in the absorbance measurement of a transparent or weakly absorbent film. The thickness and refractive index of the film can be obtained analyzing its interference maxima and minima, being the number of them proportional to the film thickness. This means there is a minimum thickness measurable using this method, which is in the range of 400-500 nm [56, 57]. Moreover, the precise localization of these maxima and minima depends on the fringe contrast, which is highly dependent on the refractive index. For instance, this contrast increases ten times as the refractive index increases from 1.5 to 2.

These mentioned limitations prevent the Swanepoel method to be used in the preparation of TFOLs, as the active film thickness varies between 150 and 1500 nm, while the resonator thickness tends to be between 50 and 200 nm. Additionally, polymeric materials commonly used present refractive index between 1.5 and 1.7, which further complicates the measurement using the Swanepoel method.

In publication 4, a new spectrophotometric method based on the Swanepoel envelope method, which is capable of measuring film thickness below 400 nm is presented. This method is based on the comparison of the experimental transmission spectrum and the one obtained by simulation at the transparent spectral window. Knowing the refractive index dispersion of the material it is possible to simulate the spectra corresponding to different values of the film thickness. Then, these can be compared to the experimental one to obtain the film thickness (Figure 3.4a). Using this method, film thickness up to 40 nm were measured keeping a 5 nm accuracy (Figure 3.4b).

The main disadvantage of the presented method is the necessity of knowing the refractive index dispersion of the analyzed material in its transparent spectral region. The final objective would be to obtain the thickness and the refractive index using the
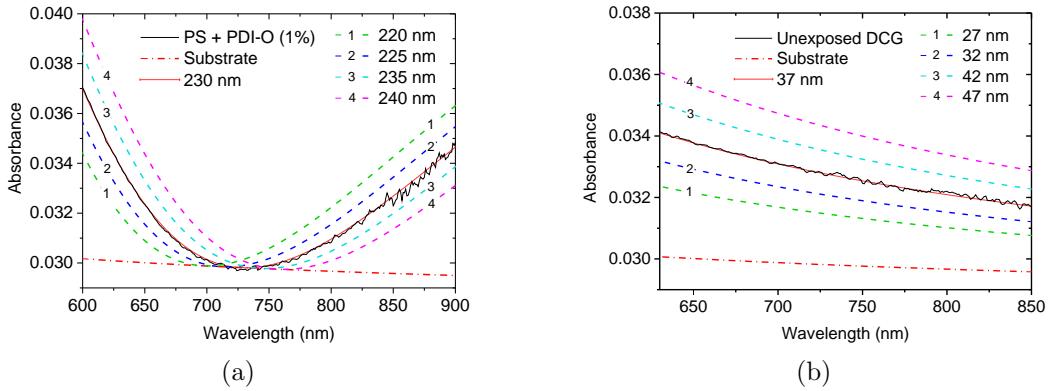
Figure 3.4: Experimental and calculated dispersion curves to measure the film thickness for (a) a 230 nm PS film doped with 1% of PDI-O; (b) a 37 nm DCG film.

spectrophotometric method, so both parameters would be variables in the simulated spectrum. However, the refractive index value at a singular wavelength is not sufficient to obtain the simulation. It is necessary to know how it changes throughout the spectral window of interest.

High transparent polymers, known as optical polymers (OP) are among the most common materials used in the fabrication of TFOLs and other optical and electronical thin-film devices. They present high transparency (over 85%) in the visible and NIR range, and they are cost-effective, mechanically flexible, and easy to process. For these materials, it is vital to perform a correct and precise thickness (h) and refractive index (n) characterization. The use of a simple and non-destructive method such as a spectrophotometric one to obtain the thickness and the refractive index dispersion would be ideal, because even for the same OP these characteristics may vary with the fabrication process or between different manufacturers.

Generally, to obtain $n(\lambda)$ it is necessary to know the value of n at different wavelengths and then relate them using an adequate equation, such as the Cauchy equation. This process could be simplified if it was only necessary to know n at a singular value of wavelength to obtain $n(\lambda)$. This would allow to get simultaneously the h and $n(\lambda)$ of a thin film, as the calculations will be reduced to two variables, $n_{\lambda 0}$ and h.

Experimental data from 16 OP reported by Sultanova et al. [58] were analyzed in publication 5. The objective was to find a general behaviour of the refractive index of the OP as the wavelength changes. By using the experimental data, we aimed to find an equation relating Δn and n valid for the vast majority of OPs. Using this equation, the method proposed in publication 4 can be applied without knowing the refractive index, as the calculation has been simplified to the obtention of two variables, $n_{\lambda 0}$ and h. This allows to study how the refractive index changes as a consequence of a change in the physical properties, such as the decrease of film thickness below 100 nm [59].

This method was successfully applied to commercial polymers (PS and PMMA),

natural biopolymers (gelatin) and dye-doped polymers (PS doped with PDI-O, TPD and FZ3). The results were checked using ellipsometry and were successful for every case, including the dye-doped polymers, with a reduced transparent spectral window of 200 nm. Accuracy decreases as the difference between the refractive indexes of the substrate and the thin film is reduced (see Figure 3.5). In our case, the refractive indexes at 633 nm were 1.45 for the FS substrate, 1.49 for PMMA and 1.59 for PS. The minimum measurable thickness is 30 nm in the case of PS and 60 nm for the PMMA. Additionally, the absolute deviations in n and h are 0.003 and 2 nm for the PS and 0.006 and 4 nm for PMMA. Note that the accuracy of the measurements of PMMA is reduced by a factor of 2 compared to PS.
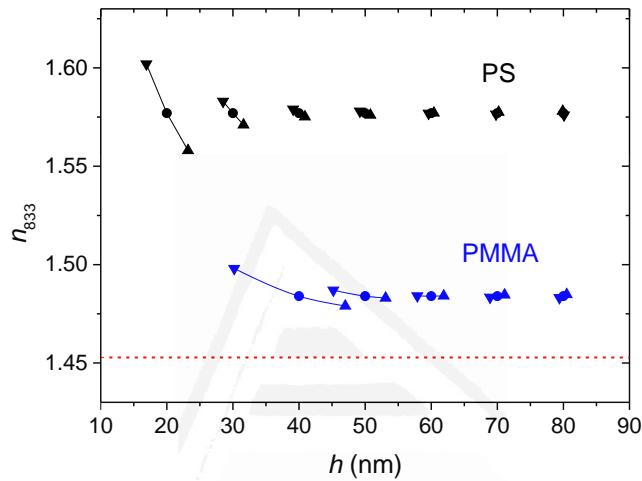

Figure 3.5: Systematic errors for simultaneous thickness and refractive index determination for PS and PMMA using the spectrophotometric method presented in publication 5

The last three publications are the ones that respond to the second objective. New materials to be used as active material in TFOLs were investigated in collaboration with different research groups. They were responsible for the design and synthesis of the compounds, as well as their chemical characterization. In publications 6, 7 and 8, wise and efficient designs of different compounds were made, which enabled the expected emission properties.

In these publications, my personal contribution was not the design and synthesis of the compounds, but the evaluation of their potential to be used as active material in TFOLs and the optimization of the devices fabricated using them, dispersed in thermoplastic polymers, as active materials.

The first example which clearly shows the advantages of the rational chemical design to control the properties of the materials is presented in publication 6, with the nanographenes FZ1, FZ2 and FZ3 (see Figure 3.6a). They are three four-zigzag edged nanographenes from the $[n,m]$peri-acenoacene family, with $n = 3$ and m growing for each nanographene, increasing their size in the same direction ($m = 2$ for FZ1, $m = 3$ for FZ2 and $m = 4$ for FZ3). These molecules were synthesized by Dr. Yanwei

Gu and Prof. Jishan Wu from the National University of Singapore. Additionally, Dr. Fernando Gordillo Gámez and Prof. Juan Casado from University of Malaga contributed with physical chemistry measurements and analysis. ASE was characterized in our group with major contributions from Dr. Pedro G. Boj and Dr. Rafael Muñoz-Mármol. My contribution in this work was focused on the fabrication and analysis of the second order DFB lasing devices. These devices were fabricated with the grating on top of the active film (RT architecture) and considering the optimization studied in publication 1. It was the first time that laser devices were fabricated with nanographenes as active material. This work increases the versatility of molecular graphenes, as they can be used not only for their magnetic and semiconductor properties but also for their light-emitting properties in devices such as organic lasers.

(a)

(b)
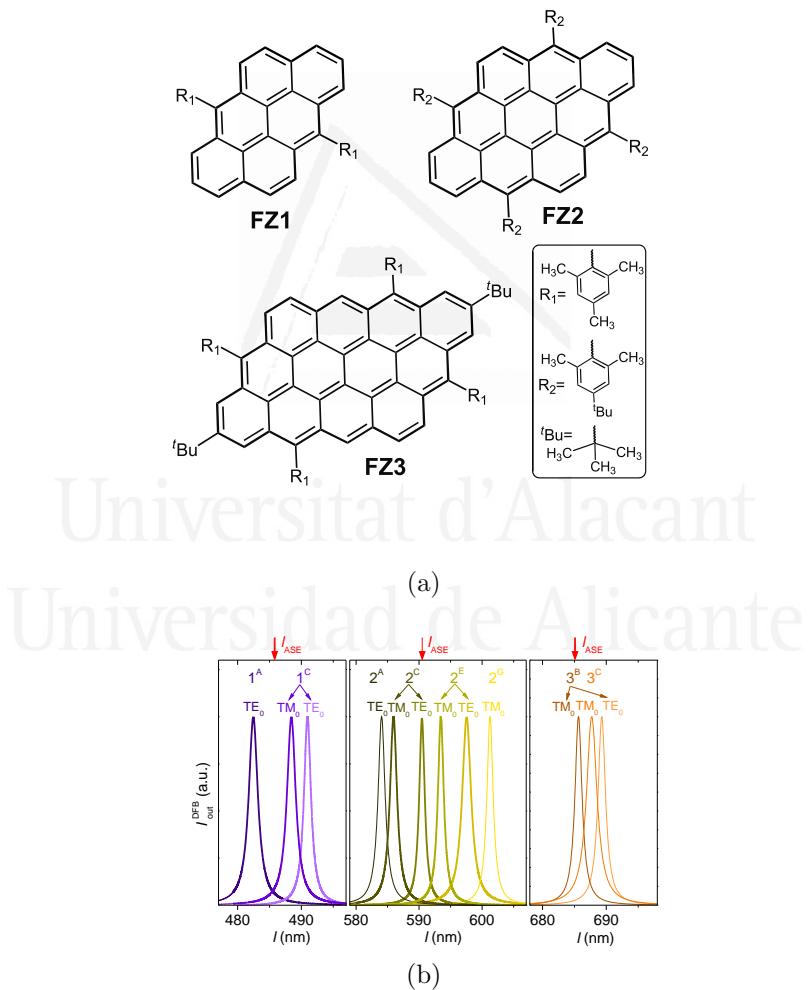
Figure 3.6: (a) Chemical structures of nanographenes FZ1, FZ2 and FZ3; (b) Emission spectra of DFB lasers based on nanographene-doped PS films.

Lasing performance of these devices was remarkable, especially in terms of their photostability, higher than 2×10^5 pump pulses for FZ2 and FZ3. They also present low lasing thresholds, with values of 11 μJ/cm^2 (3 kW/cm^2) for FZ2. Moreover, the

redshift of the emission wavelength with the increasing size of the nanographene was also observed in solution and in solid state. In the final second order DFB laser devices, the emission range was between 482 nm and 495 nm for FZ1, between 584 nm and 601 nm for FZ2 and between 674 nm and 689 nm for FZ3.

Another family of compouns, analyzed in publication 7, are aggregation-free poly-cyclic aromatic hydrocarbons (PAH) with partial zigzag periphery known as ZY-01, ZY-02, and ZY-03 (see Figure 3.7a). The chemical design and synthesis were carried out again by Prof. Jishan Wu et al. and the physical chemistry measurements were performed by Prof. Juan Casado et al.

PAH with a large size and disk form have been selected for different applications thanks to their effective charge transport, which is a consequence of their strong $\pi - \pi$ stacking along the self-assembled columnar superstructures. Nevertheless, this means the aggregation usually quenches the PL, preventing their use in solid-state light-emitting devices. To solve this issue, long alkyl or alkylphenyl chains were incorporated into the molecules to improve their solubility and prevent PL quenching (although not but completely). Importantly, their PLQY is strongly determined by their edge structure. All-armchais-edged PAH present PLQY lower than 3% in solution due to the simetrically forbidden electronic transitions,while PAH with two or more zigzag type peripheries have a smaller gap and an improved PLQY. A great example of this are the nanographenes reported in publication 6, as they are PAH with four zigzag edges, which show excellent optical properties, including high PLQY values.

Here, aggregation-free PAH with partial zigzag edges mean the development of a new strategy towards large-size aggregation-free PAH which can be used in organic lasers. During the synthesis process, perylene, one of the most used dyes in organic lasers was used. Its structure has two zigzag edges at the peri termini and the major drawback of this molecule is its tendency to aggregate. A new cyclopenta (CP) ring was developed using a fused perylene as building block (CP-Per), which allowed the synthesis of a series of free extended rylenes (CP-Rylene) with increased solubility and low aggregation. The materials presented in publication 7 are the partially fused ZY-01 and ZY-03 and the totally fused ZY-02 and ZY-04. Peripherical CP-rings completely prevents $\pi - \pi$ intermolecular interactions, which are critical to efficient luminescence in solid state. It could also be checked by X-Ray analysis that these molecules present large intramolecular distances, which helps to reduce their aggregation.

The emission properties of compounds ZY-01, ZY-02 and ZY-03 were studied, obtaining similar electronic structures and optical properties then those of the perylene family, with high PLQY. ZY-03 has a twisted backbone and did not show ASE or lasing, most probably due to the presence of non-radiative processes such as internal conversion or intersystem crossing. On the contrary, ZY-01 and ZY-02 have an almost planar backbone, showing ASE and lasing properties at concentrations up to 6 wt% in PS for ZY-01 ($\lambda_{ASE} \sim 515$ nm) and up to 3 wt% in PS for ZY-02 ($\lambda_{ASE} \sim 570$ nm).
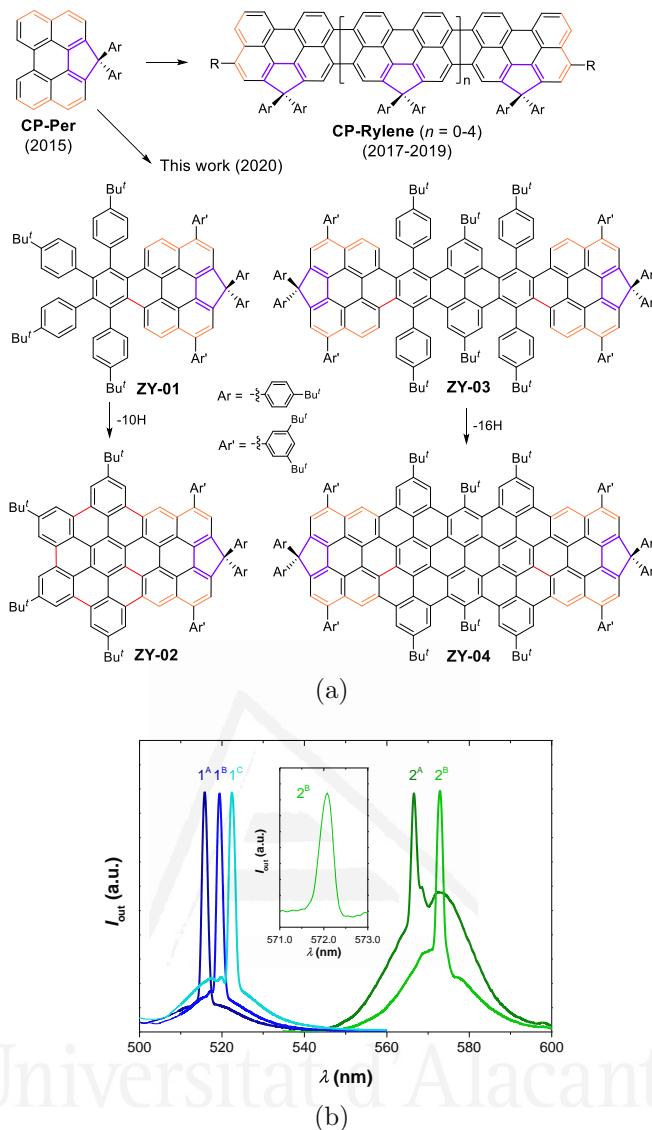
Figure 3.7: (a) Chemical structures of the perylene-fused PAH ZY-01, ZY-02, ZY-03 and ZY-04; (b) Emission spectra of DFB lasers based on nanographene-doped PS films doped with ZY-01 and ZY-02

The fabricated DFB laser devices also present tunable emission, in the range 515-523 nm for ZY-01 and 566-572 nm for ZY-02 (Figure 3.7b), with very narrow linewidths (0.36 nm in the spectra shown in the inset of Figure 3.7b).

Lastly, some new carbon-bridged oligo(p-phenylenevinylene)s derivatives were studied in publication 8, specifically of COPV1 and COPV2 [31]. COPVn with n higher than 3 present great optical properties as active material for organic lasers, as they have low lasing thresholds and an exceptional photostability. However, the blue-emitting shorter compounds COPV1 and COPV2 do not have those attributes, particularly in terms of their photostability, because of their reactive terminal sites in the photoexcited states. The new derivatives were designed and synthesized by Shoya Watanabe and Prof. Hayato Tsuji from Kagawa University and Dr. Naiti Lin anf Prof. Eiichi

Nakamura from University of Tokyo. These were designed with the aim of preventing photodegradation and improving the stability. These were accomplished through the functionalization of the terminal sites of COPV1 and COPV2 with two types of sterically bulky protective substituents: Tip (2,4,6-triisopropylphenyl) and tertbutyl (*t*-Bu) groups. Additionally, the efficacy of the stabilization using the kinetic isotope effect was examined for COPV2, adding deuterium in the terminal sites. Considering the different strategies, the final derivatives studied were: COPV1-Tip, COPV1-*t*-Bu, COPV2-Tip, COPV2-*t*-Bu y COPV2-d_2 (Figure 3.8a).

(a)

(b)
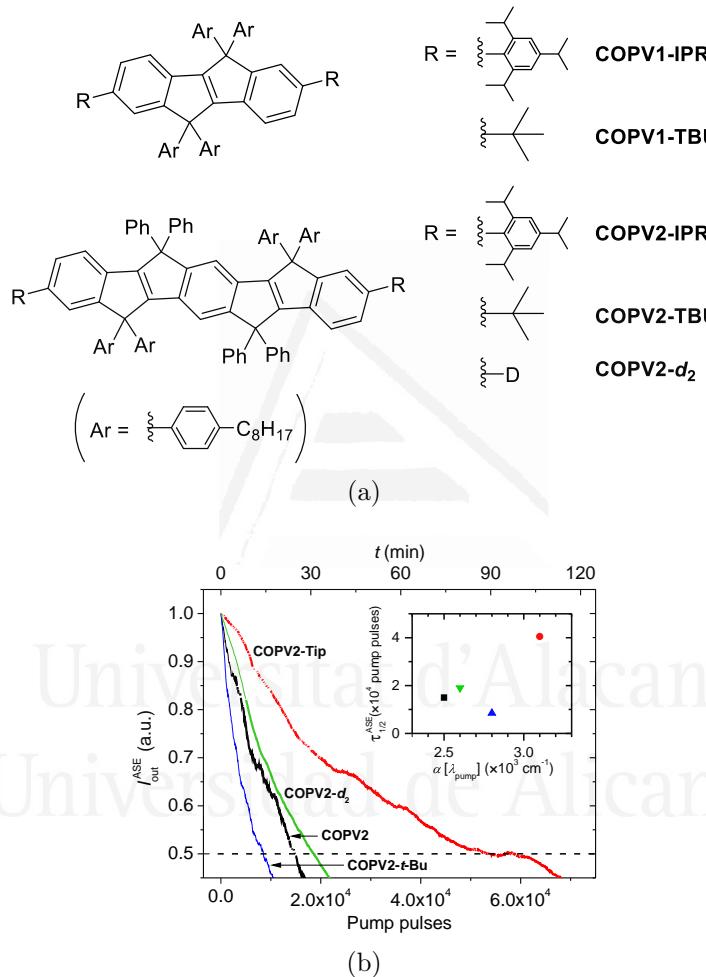
Figure 3.8: (a) Chemical structures of the COPV1 and COPV2 derivatives studied in publication 8; (b) Photostability comparison between COPV2 and its newly synthesized derivatives.

PS films doped with all the derivatives were fabricated to study the emission properties, focusing on the different strategies to prevent photodegradation. The compounds with Tip substituents were 3 times more stable than the original molecules (see Figure 3.8b), while the ones with the t-Bu substituents presented a lower stability than the original ones. The stabilization using the kinetic isotope effect was not proven to be effective, so the terminal atom H(D) does not play a major role in the degradation process.

Lasing thresholds were kept constant for each family if the absorption effect is considered, except for COPV1-*t*-Bu, which presented a clearly higher threshold. Moreover, every substituent has the additional feature of modifying the ASE wavelength, which ranged between 385 nm and 413 nm for the COPV1 derivatives and between 462 nm and 474 nm for the COPV2 ones.

All these compounds have been used as an active material in the fabrication of blue emitting organic lasers presented in publication 2. An additional COPV1 derivative was synthetized, named as COPV1(Me)-*t*-Bu, following the same strategies to tune the emission wavelength to a lower value then that of the original compound. This new derivative showed ASE at 374 nm, allowing us to prove the efficacy of the top-layer DCG resonators to fabricate deep-blue emitting lasers.

3.4 Justification of the thematic coherence

In section II, the main results from each one of the published works has been presented. All these results are included in at least one of the objectives proposed in section 3.1.

The first objective refers to the publications 1, 2, 3, 4 and 5, as all of them aim to optimize the DFB laser devices. The first three publications achieve that goal through the resonator optimization, leading to: i) to an improved threshold and efficiency, for publication 1; ii) an extension of the range of operation of the devices, enabling emission in the deep-blue region of the spectrum, for publication 2; and iii) to determine the effect of using the resonator on top or below the active film, in publication 3. Meanwhile, the publications 4 y 5 focus their attention in the determination of the thickness and refractive index of thin films using non-destructive and simple spectrophotometric methods. This allowed the precise characterization of all the films used in the DFB laser devices (active films and DCG layers) and therefore the optimization of the fabrication process.

The publications 6, 7 and 8 are included in the second proposed objective, dealing with the study of new organic molecules to be used as active material in TFOLs. These three publications analyze the emission characteristics of three different families of compounds and their use as active materials in DFB lasers. Publication 2 can also be partially included in this objective, as it presents devices made with the materials studied in publication 8 and also includes a new derivative with UV emission.

Part II

Publications

Publication 1

Controlling the emission properties of solution-processed organic distributed feedback lasers through resonator design

V. Bonal, J. A. Quintana, J. M. Villalvilla, P. G. Boj,

M. A. Díaz-García

Abstract: Surface-emitting distributed feedback (DFB) lasers with both, resonator and active material based on solution-processable polymers, are attractive light sources for a variety of low-cost applications. Besides, the lasers should have competitive characteristics compared to devices based on high-quality inorganic resonators. Here, we report high performing all-solution-processed organic DFB lasers, consisting of water-processed photoresist layers with surface relief gratings located over the active films, whose emission properties can be finely tuned through resonator design. Their laser threshold and efficiency are simultaneously optimized by proper selection of residual resist thickness and grating depth, d. Lowest thresholds and largest efficiencies are obtained when there is no residual layer, while a trade-off between threshold and efficiency is found in relation to d, because both parameters decrease with decreasing d. This behaviour is successfully explained in terms of an overlap factor r, defined to quantify the interaction strength between the grating and the light emitted by the active film and traveling along it, via the evanescent field. It is found that optimal grating depths are in the range 100–130 nm ($r \sim 0.5$-0.4). Overall, this study provides comprehensive design rules towards an accurate control of the emission properties of the reported lasers.

Publication 2

Blue and deep-blue-emitting organic lasers with top-layer distributed feedback resonators

V. Bonal, J. M. Villalvilla, J. A. Quintana, P. G. Boj, N. Lin,
S. Watanabe, K. Kazlauskas, O. Adomeniene, S. Jursenas, H. Tsuji,
E. Nakamura, M. A. Díaz-García

Abstract: All-solution processed surface-emitting organic distributed feedback lasers are attractive devices for low-cost applications. Here, lasers emitting in the spectral region between 375 and 475 nm, in which both active material and resonator (1D relief gratings) are based on solution-processable polymer films, are reported. Ten different organic compounds dispersed in polystyrene are used as active layers of the prepared devices. They include various carbon-bridged oligo(p-phenylenevinylene) (COPVn, with n = 1,2) derivatives and two terfluorene compounds. The synthesis and complete optical and amplified spontaneous emission properties of one of the COPV1 compounds, COPV1(Me)-t-Bu, designed for deep-blue emission, are also included. The feasibility of the resonator fabrication, performed by holographic lithography with a dichromated gelatine photoresist over the active film, is successfully demonstrated for all devices. Remarkably, no resolution limitations are found even for the lowest grating period (235 nm) required for the fabrication of the laser based on COPV1(Me)-t-Bu. It is also demonstrated that the rectangular grating profile with duty cycle 0.75:0.25 (hill:valley) is very convenient to optimize the resonator efficacy.

Publication 3

N,N'-Bis(3-methylphenyl)-N,N'-dyphenylbenzidine based distributed feedback lasers with holographically fabricated polymeric resonators

V. Bonal, J. A. Quintana, J. M. Villalvilla, P. G. Boj,
R. Muñoz-Mármol, J. C. Mira-Martínez, M. A. Díaz-García

Abstract: The molecule *N,N'*-bis(3-methylphenyl)-*N,N'*-dyphenylbenzidine (TPD) has been widely used in optoelectronic applications, mainly for its hole-transporting properties, but also for its capability to emit blue light and amplified spontaneous emission, which is important for the development of organic lasers. Here, we report deep-blue-emitting distributed feedback (DFB) lasers based on TPD dispersed in polystyrene (PS), as active media, and dichromated gelatin layers with holographically engraved relief gratings, as laser resonators. The effect of the device architecture (with the resonator located below or on top of the active layer) is investigated with a dye (TPD) that can be doped into PS at higher rates (up to 60 wt%), than with previously used dyes (<5 wt%). This has enabled changing the index contrast between film and resonator, which has an important effect on the laser performance. With regards to thresholds, both architectures behave similarly for TPD concentrations above 20 wt%, while for lower concentrations, top-layer resonator devices show lower values (around half). Remarkably, the operational durability of top-layer resonator devices is larger (in a factor of around 2), independently of the TPD concentration. This is a consequence of the protection offered by the resonator against dye photo-oxidation when the device is illuminated with pulsed UV light.

Publication 4

Sub-400 nm film thickness determination from transmission spectra in organic distributed feedback lasers fabrication

V. Bonal, J. A. Quintana, R. Muñoz-Mármol, J. M. Villalvilla, P. G. Boj, M. A. Díaz-García

Abstract: The design and fabrication of thin-film based organic optoelectronic devices require knowledge of the film optical properties. A low-cost and non-destructive method often used for optical characterization of films is the well-established spectrophotometric envelope method. However, this method is typically limited to thickness above 400 nm, a value often higher than that of the films involved in these devices. This paper studies a procedure to obtain the thickness of sub-400 nm active films from their spectrophotometric trace when the refractive index is previously known. The proposed procedure is based on comparing the experimental transmission spectrum in the transparent spectral window with that obtained by simulation. The capabilities of the proposed method are demonstrated here by its application in the fabrication of organic distributed feedback lasers, for which a fine control of film thickness is important to obtain an optimized and reproducible response. Results are verified with other techniques, such as ellipsometry and profilometry. Thus, with the proposed method, film thickness can be easily determined down to 40 nm maintaining an accuracy of about 5 nm even for films with low refractive index (1.5–1.7). Different methods to determine refractive index of these films are also discussed.

Publication 5

Simultaneous determination of refractive index and thickness of submicron optical polymer films from transmission spectra

V. Bonal, J. A. Quintana, J. M. Villalvilla, R. Muñoz-Mármol,

J. C. Mira-Martínez, P. G. Boj, M. E. Cruz, Y. Castro,

M. A. Díaz-García

Abstract: High-transparency polymers, called optical polymers (OPs), are used in many thin-film devices, for which the knowledge of film thickness (h) and refractive index (n) is generally required. Spectrophotometry is a cost-effective, simple and fast non-destructive method often used to determine these parameters simultaneously, but its application is limited to films where $h > 500$ nm. Here, a simple spectrophotometric method is reported to obtain simultaneously the n and h of a sub-micron OP film (down to values of a few tenths of a nm) from its transmission spectrum. The method is valid for any OP where the n dispersion curve follows a two-coefficient Cauchy function and complies with a certain equation involving n at two different wavelengths. Remarkably, such an equation is determined through the analysis of n data for a wide set of commercial OPs, and its general validity is demonstrated. Films of various OPs (pristine or doped with fluorescent compounds), typically used in applications such as thin-film organic lasers, are prepared, and n and h are simultaneously determined with the proposed procedure. The success of the method is confirmed with variable-angle spectroscopic ellipsometry.

Publication 6

Solution-processed nanographene distributed feedback lasers

V. Bonal, R. Muñoz-Mármol, F. Gordillo Gámez, M. Morales-Vidal,
J. M. Villalvilla, P. G. Boj, J. A. Quintana, Y. Gu, J. Wu, J. Casado,
M. A. Díaz-García

Abstract: The chemical synthesis of nanographene molecules constitutes the bottom-up approach toward graphene, simultaneously providing rational chemical design, structure-property control and exploitation of their semiconducting and luminescence properties. Here, we report nanographene-based lasers from three zigzag-edged polycyclic aromatics. The devices consist of a passive polymer film hosting the nanographenes and a top-layer polymeric distributed feedback resonator. Both the active material and the laser resonator are processed from solution, key for the purpose of obtaining low-cost devices with mechanical flexibility. The prepared lasers show narrow linewidth (<0.13 nm) emission at different spectral regions covering a large segment of the visible spectrum, and up to the vicinity of the near-infrared. They show outstandingly long operational lifetimes (above 10^5 pump pulses) and very low thresholds. These results represent a significant step forward in the field of graphene and broaden its versatility in low-cost devices implying light emission, such as lasers.

Publication 7

Perylene-fused, aggregation-free polycyclic aromatic hydrocarbons for solution-processed distributed feedback lasers

Y. Zou, **V. Bonal**, S. Moles Quintero, P. G. Boj, J. M. Villalvilla,
J. A. Quintana, G. Li, S. Wu, Q. Jiang, Y. Ni, J. Casado,
M. A. Díaz-García, J. Wu

Abstract: Perylene-fused, aggregation-free polycyclic aromatic hydrocarbons with partial zigzag periphery (**ZY-01**, **ZY-02**, and **ZY-03**) were synthesized. X-ray crystallographic analysis reveals that there is no intermolecular π–π stacking in any of the three molecules, and as a result, they show moderate-tohigh photoluminescence quantum yield in both solution and in the solid state. They also display the characteristic absorption and emission spectra of perylene dyes. **ZY-01** and **ZY-02** with a nearly planar π-conjugated skeleton exhibit amplified spontaneous emission (ASE) when dispersed in polystyrene thin films. Solution-processed distributed feedback lasers have been fabricated using **ZY-01** and **ZY-02** as active gain materials, both showing narrow emission linewidth (<0.4 nm) at wavelengths around 515 and 570 nm, respectively. In contrast, **ZY-03** did not show ASE and lasing, presumably due to its highly twisted backbone, which facilitates nonradiative internal conversion and intersystem crossing.

Publication 8

Kinetically protected carbon-bridged oligo(p-phenylenevinylene) derivatives for blue color amplified spontaneous emission

V. Bonal, M. Morales-Vidal, P. G. Boj, J. M. Villalvilla, J. A. Quintana, N. Lin, S. Watanabe, H. Tsuji, E. Nakamura, M. A. Díaz-García

Abstract: Carbon-bridged oligo(p-phenylenevinylene)s (COPVn with repeating unit $n = 16$) have demonstrated great success as laser dyes for thin-film organic lasers. The excellent photostability observed in the longer homologues is, however, not present in the blue-emitting shorter compounds COPV1 and COPV2, attributed to the unprotected terminal positions that can degrade by photoreaction in the excited state. Here we report the synthesis of various COPV1 and COPV2 derivatives functionalized at the terminal positions with two types of sterically bulky protecting substituents: Tip (2,4,6-triisopropylphenyl) and *tert*-butyl (t-Bu) groups. Such molecular designs aim at preventing such photodegradation processes and thus to improve their stability. The efficacy of kinetic isotope effect for stabilization is also examined for COPV2, by the addition at terminal positions of deuterium atoms. Absorption, photoluminescence (PL), including PL quantum yield, and amplified spontaneous emission (ASE) studies have been conducted in polystyrene films doped with each of the derivatives. Significant and slight improvements of the ASE photostability are observed for the compounds with Tip groups and deuterium, respectively. Installation of substituents slightly affects the ASE wavelength within the blue spectral region, that is 385-413 nm and 462-474 nm, for COPV1 and COPV2, respectively.

Conclusions

- **A fine control of the fabrication and geometrical parameters of the resonator in DFB lasers is crucial to obtain optimized performance** The influence of the residual photoresist layer and the grating depth in top-layer resonator DFB laser was studied. The results showed that the lowest laser threshold and highest laser slope efficiency correspond to devices with no residual layer. With regards to the grating depth, low values improve the threshold but decreases the efficiency. A grating depth in the range 100-130 nm provides a comprise situation: threshold $< 25~\mu\mathrm{J/cm^2}$ and the laser efficiency at 80% of its maximum possible value. The observed behavior was interpreted in terms of the overlap between the electric field intensity distribution and the grating. Additionally, the new simplified dry development method using an inexpensive plasma cleaner machine was proven to be successful, as the resulting DFB lasers presented a good performance and quality.

- **DFB lasers with DCG resonators on top of the active film have proven to be successful for blue and deep-blue emitting devices (spectral region between 375 and 475 nm).** No resolution limitations were found even for the lowest grating period (235 nm) required for the fabrication of the deep-blue emitting lasers. Besides, it was also demonstrated that the rectangular grating profile with duty cycle 0.75:0.25 (hill:valley) is very convenient to optimize the resonator efficacy because it balances the feedback and the losses in these devices. These optimized gratings were tested fabricating DFB devices with multiple blue-emitting molecules as active materials. Among them, a new COPV1 derivative, COPV1-Me-*t*-Bu was synthetized and characterized. This is the COPV1 derivative emitting at a shorter wavelength (374 nm), which extended the use of this optimized devices into the UV.

- **In DFB lasers based on DCG resonators, the top-layer resonator (RT) configuration (RT) presents various advantages over the bottom-layer resonator one (RB).** These two configurations were tested using TPD as active material, which can be doped at high rates into the matrix (PS), which provides a way to tune the refractive index of the active layer, and therefore the effective index. For high TPD concentrations ($> 20\,\mathrm{wt\%}$), both configurations

showed similar threshold, but for lower concentrations the threshold was lower in the RT configuration due to a better electric field confinement in the active layer. In terms of photostability, it was better in the RT-type devices (by two times) attributed to the protection against dye photo-oxidation under UV-light illumination, offered by the location of the resonator above the active film.

- **Film thickness below 500 nm can be measured with the new developed spectrophotometric method.** The accuracy of the results obtained for films of tenths of nm for low refractive indexes (1.5-1.7) are comparable to the ones obtained with the well-known envelope method for 1 μm films with a refractive index value of 3. Additionally, in the case of the optical polymers (OP), widely used in the organic laser field, the method allows for simultaneous determination of the refractive index and the film thickness. A collection of OPs was analysed to find an optical general behaviour for them, which allowed to reduce the refractive index dispersion determination to just one variable. This implies significant savings in work and time because no external procedures to measure the refractive index was needed. The accuracy of the method depends on the similarity between the refractive index of film and substrate. In the case of PS and PMMA (indices of 1.59 and 1.49 respectively) deposited over a FS substrate (index of 1.45), the minimum measurable thickness is around 30 nm, for PS, and 60 nm, for PMMA. The errors in index and thickness were respectively 0.003 and 2 nm, for PS; and 0.006 and 4 nm for PMMA

- **DFB lasers based on nanographenes were reported for the first time. The fabrication of DFB lasers using nanographenes FZ1, FZ2 and FZ3 as active materials proved the great potential of these materials for lasing applications.** These nanographenes derive from anthanthrene and are characterized for having four zigzag edges, with changes in their ASE mechanism as they vary in molecular size, with ASE wavelengths of 486 nm, 590 nm, and 685 nm for FZ1, FZ2 and FZ3, respectively. They present outstanding chemical stability and against photodegradation, with operational times for FZ2 and FZ3 larger than 2×10^5pump pulses. Additionally, they were able to work as an active waveguide in DFB lasers dispersed in polymeric matrices at very low concentrations (1 wt%), preventing molecular interactions and reactions that could potentially quench their photoluminescence characteristics and therefore maintaining low laser threshold values compared to other organic dyes.

- **The synthesis of large-size aggregation-free PAHs from a CP-ring fused perylene building block was developed with good characteristics to be used in organic laser devices.** They presented an efficient solid-state luminescence thanks to the suppression of π-π interactions in the periphery due to the presence of CP-rings. The perylene-fused aggregation-free PAHs ZY-01 and ZY-02 have a nearly planar π-conjugated skeleton, which allows the PS films

doped with them to exhibit ASE. This led to the fabrication of efficient DFB laser devices with tuneable emission wavelengths around 515 nm and 570 nm respectively. On the contrary, ZY-03 presented a twisted backbone and therefore did not show ASE or lasing behaviour.

- **The addition of the sterically bulky protecting substituents Tip (2,4,3-triisopropylphenyl) to the terminal positions of COPV1 and COPV2 was found to be a successful strategy to improve their operational ASE lifetime.** The lifetime was three times better with these derivatives than with the original COPV1 and COPV2 molecules. Some other substituents and effects were not successful in the objective of improving the photostability of the compounds. The derivatives with the tert-butyl substituent presented lower photostability and higher threshold values, and the COPV2-d_2 with deuterium atoms at terminal positions did not improve the photostability either, proving that the terminal H atom is not the rate-determining step of the degradation process. Even if all these strategies were not valid for the main objective of increasing the photostability, they did provide a useful side effect that can be exploited, the ASE wavelength tunning by the addition of new substituents. These ASE wavelengths changed between 385 nm and 413 nm for the COPV1 derivatives and between 462 and 474 nm for the COPV2 derivatives.

Resumen y conclusiones

En esta sección se muestra un resumen de los resultados obtenidos y las conclusiones. Esta tesis ha sido realizada por compendio de publicaciones, así que para obtener más información se recomienda la lectura de dichas publicaciones en la parte II.

Objetivos

El objetivo de este trabajo es la optimización de los láseres DFB basados en resonadores difractivos poliméricos, preparados como una capa independiente y situados encima de la capa activa (arquitectura conocida como "top-layer resonator" o RT). Esto se divide en dos objetivos principales:

a) Optimización del resonador mediante el control de los parámetros de fabricación y geométricos para mejorar el rendimiento de los láseres DFB.

b) El diseño y fabricación de láseres DFB optimizados para nuevas moléculas orgánicas utilizadas como material activo

En primer lugar, para optimizar el resultado de los dispositivos, se realizó un estudio sistemático de la influencia de diversos parámetros en la fabricación de las redes (espesor inicial de la capa, tiempo de exposición, tiempo de revelado. . .), analizando su influencia en las propiedades de emisión finales de los dispositivos láser DFB con el resonador sobre la capa activa. Además, se estudió la capacidad del material usado en la fabricación de las redes (gelatina dicromatada, DCG) para fabricar láseres con emisión a menores longitudes de onda. Por último, esta arquitectura de láseres DFB se comparó con las utilizadas habitualmente para comprobar la mejora de su rendimiento.

Después de esta optimización del resonador, se fabricaron redes y láseres DFB adecuados para diferentes materiales activos. Se estudiaron diversas familias de compuestos con síntesis novedosa en el contexto químico, cuyas longitudes de onda de emisión cubrieron desde el ultravioleta hasta el infrarrojo cercano.

Principales resultados

Como se ha explicado en la sección anterior, el primer objetivo de esta tesis es la optimización de los dispositivos láseres DFB con el resonador encima de la capa activa. Para ello, en primer lugar, se ha estudiado la influencia de las características del resonador en las propiedades de emisión de los dispositivos en la publicación 1. En este tipo de dispositivos, la capa activa presenta un espesor uniforme al estar situado el resonador sobre la misma. Esto tiene ciertas ventajas en términos del umbral y de la eficiencia (LSE) de los dispositivos, pero además permite modificar las características de emisión únicamente con variaciones de los distintos parámetros geométricos del resonador, sin que esto afecte a la capa activa. En nuestro caso, hemos centrado nuestra atención en dos parámetros: el espesor de la capa residual (que separa la capa activa y la red) y la modulación de la red de relieve.

Además, en el proceso de fabricación de la red se ha utilizado un nuevo sistema de revelado seco, utilizando un plasma de oxígeno producido por una máquina sencilla de tratamiento de superficies. Esto, sumado a que tanto la capa activa como el resonador se fabrican a partir de disolución, proporciona un proceso de fabricación sencillo, económico y fácilmente escalable.

En la Figura 3.1, se analiza el efecto de la capa residual y de la modulación en dos de los parámetros más importantes a la hora de caracterizar la emisión láser, como son el umbral láser y la LSE. Se muestran curvas para distintos espesores iniciales de DCG con distintos tiempos de revelado. De esta manera, para cada curva, conforme aumenta el tiempo de revelado, aumenta su modulación y disminuye su capa residual, hasta que la capa residual se hace nula (marcado con líneas discontinuas). Los resultados obtenidos muestran, en primer lugar, que los dispositivos con menor capa residual presentan tanto menor umbral como una mayor eficiencia, de modo que podemos concluir que la contribución de la capa residual es negativa para los dos parámetros estudiados. En cuanto a la modulación, se puede ver que el análisis no es tan sencillo, ya que tanto el umbral como la eficiencia aumentan con la modulación, así que hay que buscar un compromiso entre ambas. Se puede observar en la figura 3.1b, que al aumentar la modulación se llega a un límite en el aumento de eficiencia, que se debe a que la red es menos eficiente cuanto mayor es su modulación. Por ello, el valor óptimo de la modulación se sitúa en el rango 100-130 nm, que tendría un umbral mejor a 25 μJ/cm^2 y una eficiencia en torno al 80 % de su valor máximo alcanzable.

A continuación, pasamos analizar las capacidades de las redes de difracción de DCG para actuar como resonadores en dispositivos laser DFB con esta arquitectura emitiendo en la zona azul del espectro visible. Hasta ese momento los dispositivos láseres DFB con esta configuración se habían realizado únicamente para materiales emitiendo en la zona del verde y del rojo del espectro visible. Para ello se han fabricado resonadores de DCG hechos mediante litografía holográfica con distintos periodos, comprobando

que no pierden resolución al bajar de periodo y que la modulación se mantiene constante desde los 500 nm hasta los 200 nm (Figura 3.2a).

Además, se ha estudiado el efecto del perfil de la red en el rendimiento de los láseres, concretamente el duty cycle de redes de relieve cuadradas a través del análisis de los coeficientes de acoplamiento (tanto κ_1 que describe las pérdidas, como κ_2, que se refiere a la realimentación). Los resultados se muestran en la Figura 3.2b para dos redes de difracción correspondientes a dos dispositivos con COPV1-Me-t-Bu y COPV2-Tip como materiales activos, emitiendo en 376 nm y 474 n, respectivamente. El duty-cycle utilizado en nuestros dispositivos se sitúa en torno al 0.75. Se puede comprobar en la Figura 3.2b que este valor maximiza la realimentación y reduce las pérdidas el mismo tiempo, por lo que es una buena elección para la optimización de los dispositivos.

Para comprobar la idoneidad de estas redes para fabricar dispositivos emitiendo en la zona azul del espectro visible, se realizan láseres de realimentación distribuida con diversos materiales que emiten en esta zona del espectro. Estos materiales fueron utilizados gracias a la colaboración del Dr. Naiti Lin y el Prof. Eiichi Nakamura (de la Universidad de Tokyo), de Shoya Watanabe y del Prof. Hayato Tsuji (de la Universidad de Kanagawa) y del Dr. Karolis Kazlauskas, del Dr. Ona Adomeniene y del Prof. Saulius Jursenas (de la Universidad de Vilnius) que proporcionaron estos materiales activos. Entre ellos, destaca el COPV1-Me-t-Bu (proporcionado por los grupos del Prof. Hayato Tsuji y del Prof. Eiichi Nakamura), material que emite ya en el ultravioleta y cuya síntesis y caracterización óptica se presenta en este trabajo. Se consiguió fabricar dispositivos láseres DFB con todos ellos, destacando principalmente la mejora en los valores del umbral para los materiales con los que ya se habían publicado anteriormente [31], permitiendo además una mejor sintonización de la longitud de onda de emisión al aprovechar la versatilidad que ofrece la litografía holográfica. Se comprueba con esto que se ha conseguido optimizar esta arquitectura para fabricar láseres DFB emitiendo en este rango, lo que abre la puerta a su utilización en diferentes aplicaciones.

Tras el análisis de las capacidades de los dispositivos DFB con el resonador sobre la capa activa (arquitectura RT), en la publicación 3 realizamos una comparación detallada con los dispositivos en los que el resonador se sitúa debajo de la capa activa (arquitectura RB). La configuración RB es muy similar a la configuración típica para este tipo de láseres, aunque en ese caso la red está grabada sobre el sustrato inorgánico [49]. El material activo utilizado en esta comparación ha sido el N,N'-bis(3-methylphenyl)-N,N'-dyphenylbenzidine, también conocido como TPD. Este material ha sido muy utilizado en aplicaciones optoelectrónicas debido a su capacidad como transportador de huecos, pero sus capacidades de emisión no han sido muy estudiadas.

Una característica importante que presenta este material es que se puede utilizar en altas concentraciones dispersado en una matriz polimérica (típicamente de poliestireno) sin que disminuya su fotoluminiscencia. De hecho, TPD muestra ASE incluso en estado sólido sin estar dispersado en una matriz inerte [52]. Esto nos va a permitir

comparar ambas configuraciones con características que no se habían podido explorar hasta el momento, ya que las capas activas utilizadas en trabajos anteriores consistían en una matriz de un polímero inerte con menos de un 5 wt % de moléculas activas dispersadas en ella. Al utilizar concentraciones bajas de moléculas dispersadas, el índice de refracción de la capa activa era prácticamente el del polímero que la formaba. Esto daba lugar a un bajo contraste de índices entre la capa activa y el resonador en los dispositivos con configuración RB. Al variar la concentración de material activo en la matriz interte, el índice efectivo de la capa activa se modifica y por tanto aumenta tanto el contraste con el resonador como el confinamiento de la luz en la guía de ondas, mejorando la eficiencia de la configuración RB.

Se han fabricado dispositivos láseres DFB en las configuraciones RB y RT con distintas concentraciones de TPD en la matriz de PS, desde el 5 wt % al 60 wt %. En la Figura 3.3, se presenta la influencia de la concentración en el umbral láser y en la fotoestabilidad. En general, se ha podido comprobar como la configuración RT presenta ciertas ventajas frente a la configuración RB. Para concentraciones superiores al 20 wt %, ambas configuraciones presentan un umbral constante de unos 180 μJ/cm^2. El umbral aumenta al disminuir la concentración, pero la diferencia entre ambas configuraciones es significativa, siendo el umbral menor para la configuración RT. El aumento del umbral al disminuir la concentración se puede explicar en términos de la absorción del material, que al estar menos concentrado es menos eficiente. Sin embargo, hay una gran diferencia entre las dos configuraciones, siendo la configuración RT la que mantiene un umbral menor para un amplio rango de concentraciones. Esto se puede explicar por el confinamiento del modo en la guía de onda, que es mayor para la configuración RT para todas las concentraciones de TPD.

Por último, la fotoestabilidad es mejor para la configuración RT para todas las concentraciones, aproximadamente el doble. El principal motivo es la acción protectora de la capa de DCG al situarse encima de la capa activa que contiene TPD, previniendo su fotooxidación al ser expuesta a luz ultravioleta.

En los TFOLs, para poder tener un buen control sobre los dispositivos fabricados, es importante poder controlar el espesor de las distintas capas para de este modo poder tener respuestas optimizadas y reproducibles. Muchos de los métodos más comúnmente utilizados para medir espesores de películas delgadas con fiabilidad son destructivos, como SEM, AFM o perfilometría. En nuestro caso consideramos de vital importancia que el método no sea destructivo, para de esta manera poder controlar los distintos pasos del proceso de fabricación y optimizar los dispositivos que sí podrán ser utilizados. Los dos métodos no destructivos principales son la elipsometría y los métodos espectrofotométricos. La primera se caracteriza por tener una gran sensibilidad, incluso para películas de unos pocos nanómetros. Los métodos espectrofotométricos tienen menos precisión y están limitados a capas de mayor espesor, pero a cambio son más económicos, el análisis es más sencillo y requieren menos tiempo.

El principal método espectrofotométrico de medida de espesores es el método de las envolventes propuesto por Manifacier en 1976 [53], también conocido como método de Swanepoel por ser quien lo desarrolló en profundidad [54,55]. Este método se basa en el análisis del patrón de interferencia que aparece al medir la absorbancia de una película delgada transparente o ligeramente absorbente. El análisis se basa en la diferencia espectral entre los distintos máximos y mínimos de interferencia. El número de máximos y mínimos es proporcional al espesor de la película, de modo que al ser necesarios unos pocos máximos y mínimos para realizar el análisis, necesariamente hay un espesor mínimo que se puede medir utilizando esta técnica, que se sitúa entre los 400 y 500 nm [56,57]. Además, la precisa localización de los máximos y mínimos de interferencia depende del contraste de las franjas, que a su vez depende fuertemente del índice de refracción. Este contraste aumenta 10 veces al pasar el índice de 1.5 a 2.

Todas estas limitaciones anteriormente mencionadas, impiden que se pueda utilizar el método de Swanepoel en la mayoría de casos en la preparación de TFOLs, ya que el espesor de las capas activas suele estar entre 150 y 1500 nm, mientras que el espesor de los resonadores se sitúa entre los 50 y 200 nm habitualmente. Además, los materiales de naturaleza polimérica típicamente utilizados tienen índices de refracción entre 1.5 y 1.7, lo que complica la medida utilizando el método de Swanepoel.

En la publicación 4, se presenta un nuevo método espectrofotométrico basado en el método de Swanepoel para la medida de espesores inferiores a los 400 nm. Este método se basa en la comparación, en la ventana espectral transparente del material, entre el espectro de transmisión experimental y el obtenido mediante simulación. Para ello es necesario conocer el índice de refracción para esas longitudes de onda del material que se va a medir y se compara el espectro experimental con uno simulado con el mismo índice pero distintos espesores (Figura 3.4a). Utilizando este método, se han llegado a medir espesores de hasta 40 nm manteniendo la precisión de 5 nm (Figura 3.4b).

El principal inconveniente de este método es precisamente que para poder llevarlo a cabo necesitamos conocer el índice de refracción del material a estudiar y su variación en el rango espectral de trabajo. Para tratar de evitar tener que conocer el índice de antemano, se podría intentar realizar las simulaciones con el espesor de las películas y el índice de refracción como variables. El problema es que para poder simular las curvas de la transmitancia necesitamos conocer no solamente el índice para una longitud de onda, sino también la variación del mismo en todo el rango espectral que se vaya a utilizar.

En el ámbito de los TFOLs y otros dispositivos ópticos y electrónicos de película delgada, unos de los materiales más utilizados son los llamados polímeros ópticos (OP). Se caracterizan por tener una alta transparencia (superior al 85 %) en el visible y NIR y presentar bajo coste, facilidad de preparación y flexibilidad mecánica. Para este tipo de materiales es muy importante caracterizar correctamente el índice de refracción (n) y el espesor de las películas (h) con gran precisión. En particular, si pudiésemos utilizar

un método sencillo y rápido como el espectrofotométrico para calcular h y n sería muy útil, ya que incluso para el mismo OP puede cambiar según el método de fabricación o la casa comercial que lo prepare.

Para calcular la $n(\lambda)$, hace falta conocer la n a varias longitudes de onda y después relacionarla utilizando alguna ecuación como la ecuación de Cauchy. Este proceso de obtención de $n(\lambda)$ se podría simplificar si únicamente fuese necesario conocer un punto de la curva y se pudiese obtener el resto de la curva utilizando una ecuación conocida. Esto permitiría obtener simultáneamente $n(\lambda)$ y h para una película delgada, ya que el cálculo se reduciría a la obtención de dos variables, $n_{\lambda 0}$ y h.

En la publicación 5, se han analizado 16 OP con precisos datos experimentales reportados por sultanova et al. [58]. El objetivo es encontrar el comportamiento general del índice de refracción con la lambda para los OP. Para ello se ha relacionado n con Δn a través de una ecuación válida para la mayoría de los OP. Con esto se puede aplicar el método estudiado en la publicación 4 sin conocer el índice de refracción, ya que el cálculo se ha simplificado a la obtención de las dos variables mencionadas, $n_{\lambda 0}$ y h. Esto además permite estudiar cambios en el índice de refracción debido a algún cambio en sus propiedades físicas, por ejemplo cuando se reduce el espesor por debajo de 100 nm [59].

El método se ha comprobado para polímeros comerciales (PS y PMMA), biopolímeros naturales (gelatina) y polímeros dopados con colorantes (PS dopado con PDI-O, TPD y FZ3). Los resultados han sido comparados los resultados con los obtenidos con elipsometría, resultando satisfactorios en todos los casos incluso en el caso de polímeros dopados en los que su ventana espectral transparente se reducía hasta únicamente 200 nm. La precisión disminuye cuando la diferencia entre la capa y el sustrato disminuye (Figura 3.5). En nuestro caso, el sustrato tenía una n633 de 1.45, el PMMA de 1.49 y el PS de 1.59. El mínimo espesor para el PS es de 30 nm pero en cambio para el PMMA es de 60 nm. Además, los errores en el índice y el espesor para el PS son de 0.003 y 2 nm para el PS, mientras que para el PMMA es de 0.006 y 4 nm. La precisión de las medidas en el PMMA se reduce en un factor 2 en comparación al PS.

Las últimas 3 publicaciones, son las que tratan de dar respuesta al segundo objetivo. Se han investigado nuevos materiales susceptibles de ser utilizados como material activo en láseres orgánicos de película delgada. Esto se ha realizado en colaboración con distintos grupos de investigación, que han sido los encargados del diseño y síntesis de estos materiales, además de su caracterización química. En las publicaciones 6, 7 y 8 podremos comprobar cómo el diseño de los diferentes materiales ha sido capaz de proporcionar las propiedades deseadas en cada caso.

Cabe destacar que en estas publicaciones mi contribución específica no ha consistido en el diseño ni en la síntesis de estos materiales, sino en la evaluación del potencial de estas moléculas para ser utilizadas como material activo y en la optimización de los dispositivos que utilizan estas moléculas como material activo dispersadas en polímeros

inertes.

El primero de estos ejemplos en los que se puede ver claramente las ventajas del diseño químico racional para controlar las propiedades de los materiales es el que se presenta en la publicación 6, con los nanografenos FZ1, FZ2 y FZ3 (Figura 3.6a). Se trata de tres nanografenos con 4 extremos zigzag de la familia [n,m]peri-acenoacene, en particular con $n = 3$ y con m creciente para cada nanografeno, es decir, que van incrementando su tamaño en una única dirección ($m = 2$ para FZ1, $m = 3$ para FZ2 y $m = 4$ para FZ3). Estos nanografenos fueron sintetizados por el Dr. Yanwei Gu y el Prof. Jishan Wu de la Universidad Nacional de Singapur. Además, el Dr. Fernando Gordillo Gámez y el Prof. Juan Casado de la Universidad de Málaga contribuyeron con medidas y análisis fisicoquímicos. La ASE se caracterizó en nuestro grupo de investigación gracias a la contribución del Dr. Pedro G. Boj y del Dr. Rafael Muñoz-Mármol. Mi contribución en este trabajo se centró en la parte de la fabricación y análisis de los dispositivos láseres DFB de segundo orden. Estos dispositivos se han realizado utilizando la arquitectura con RT explicada anteriormente y aprovechando la optimización de la publicación 1. Esto supuso la primera vez que se realizaban dispositivos láseres con nanografenos como material activo, lo que amplía la versatilidad de los grafenos moleculares, ya que no solo se pueden utilizar por sus propiedades semiconductora o magnéticas, sino que también en sistemas basados en la emisión de luz como los láseres.

El rendimiento de los láseres fabricados es muy destacable, especialmente en términos de su fotoestabilidad, superior a los 2×10^5 pump pulses para el FZ2 y el FZ3. Los umbrales son también bastante buenos, llegando a valores tan bajos como $11\mu J/cm^2$ ($3\ kW/cm^2$) para el FZ2. Además, se comprueba el desplazamiento de la longitud de onda de emisión hacia el rojo al aumentar el tamaño de los nanografenos que ya se había visto al medir las propiedades ópticas de las películas tanto en disolución como en estado sólido. En el caso de los dispositivos preparados, el FZ1 emite en el rango 482-495, el FZ2 en el rango 584-601 y el FZ3 en el rango 674-689 nm.

Los siguientes materiales, analizados en la publicación 7, son una serie de hidrocarburos aromáticos policíclicos (PAH) sin agregación con periferia parcial en zigzag a partir de perilenos, denominados ZY-01, ZY-02 y ZY-03 (ver Figura 3.7a). Como en el caso anterior, el diseño y síntesis de estos materiales se llevo a cabo por el Prof. Jishan Wu et al. y las medidas químico-físicas han sido realizadas por el Prof. Juan Casado et al.

Los PAH de gran tamaño y con forma de disco se han considerado materiales interesantes para distintas aplicaciones al ser buenos transportadores de carga debido a su fuerte apilamiento $\pi - \pi$ en las superestructuras en forma de columna autogeneradas. Sin embargo, esto implica agregación que disminuye la PL, lo que lo que limita su aplicación en dispositivos emisores de luz en estado sólido. Para solucionarlo, se le suelen agregar cadenas largas de alkyl o alkylphenyl, con lo que se consigue aumentar su solubilidad e impedir la disminución de su PL (aunque no completamente). La

PLQY además viene dada por su estructura de borde. Los PAH con todos sus bordes "armchair" tienen PLQY menores al 3 % en disolución, debido a las transiciones electrónicas prohibidas por simetría y los PAH con 2 o más bordes zigzag tienen un gap menor y una PLQY mejorada. Un buen ejemplo son los materiales reportados en la publicación 6, que son PAH con 4 bordes zigzag cada uno y han mostrado unas excelentes propiedades ópticas, incluyendo un alto valor de la PLQY.

En este caso, los PAH sin agregación y con bordes parcialmente en suponen el desarrollo de una nueva estrategia hacia PAH de gran tamaño sin agregación que pueden ser utilizados como material activo en láseres orgánicos. En el proceso de síntesis se ha utilizado otro de los colorantes más usados en los láseres tradicionales, el perileno. Su estructura tiene dos bordes zigzag en las posiciones "termini" y uno de sus principales inconvenientes también es la tendencia a la agregación. Se ha desarrollado una nueva molécula a partir de perileno y anillos de ciclopentano (CP-Per) que se ha usado para sintetizar una serie de rylenes de gran tamaño (CP-Rylene) que son solubles y no presentan agregación. Los materiales presentados en la publicación 7 son los parcialmente fusionados ZY-01/ZY-03 y los totalmente fusionados ZY-02/ZY-04. Los anillos CP en las periferias suprimen completamente las interacciones $\pi - \pi$ intermoleculares, que son críticas para tener una luminiscencia eficiente en estado sólido. Mediante análisis de rayos X se puede comprobar que estos compuestos presentan grandes distancias intramoleculares, lo cual dificulta la agregación.

Se han estudiado las propiedades de emisión para los compuestos ZY-01, ZY-02 y ZY-03. Los tres PAH obtenidos muestran estructuras electrónicas y propiedades ópticas típicas de los perilenos, comuna alta PLQY. El ZY-03 tiene una estructura torcida y no presenta ASE ni láser, presuntamente debido a la existencia de procesos no radiativos IC y ISC que interfieren. En cambio, los compuestos ZY-01 y ZY-02, con una estructura prácticamente plana, muestran propiedades ASE y se han fabricado láseres DFB con longitud de onda sintonizable. El ZY-01 presenta buenos valores de PLQY y emisión ASE ($\lambda_{ASE} \sim 515$ nm) hasta una concentración del 6wt % disperso en PS y el ZY-02 ($\lambda_{ASE} \sim 570$ nm) hasta el 3 wt %. Los dispositivos láseres DFB presentan sintonizabilidad en el rango de emisión de la ASE, emitiendo en el rango 515-523 nm para el ZY-01 y en el rango 566-572 nm para el ZY-02 (Figura 3.7b), con un ancho de banda muy estrechos (0.36 nm en el espectro mostrado en el inset de la Figura 3.7b).

Por último, se han investigado también nuevos derivados de carbon-bridged oligo(p-phenylenevinylene)s en la publicación 8 , en concreto de COPV1 y COPV2 [31]. Los COPVn con n superior a 3 tienen muy buenas propiedades como material activo para láseres orgánicos, ya que tienen bajos umbrales y excepcionales fotoestabilidades. No obstante, este comportamiento no es replicado por los compuestos más cortos con emisión en el azul, COPV1 y COPV2, especialmente en lo referido a la fotoestabilidad debido a los sitios terminales reactivos en los estados fotoexcitados. Los nuevos deri-

vados fueron diseñados y sintetizados por Shoya Watanabe y el Prof. Hayato Tsuji de la Universidad de Kanagawa y por el Dr. Naiti Lin y el Prof. Eiichi Nakamura de la Universidad de Tokyo. Estos nuevos derivados pretenden prevenir la fotodegradación y mejorar la estabilidad mediante la funcionalización de las posiciones terminales de COPV1 y COPV2 con dos tipos de sustituyentes protectores: los grupos Tip (2,4,6-triisopropylphenyl) y tertbutyl (t-Bu). Además, para el COPV2, se examinó la eficacia para la estabilización del efecto de isótopo cinético, añadiendo deuterio en las posiciones terminales. Teniendo todas las estrategias en cuenta, los derivados finales a estudiar fueron: COPV1-Tip, COPV1-t-Bu, COPV2-Tip, COPV2-t-Bu y COPV2-d_2 (Figura 3.8a).

Se fabricaron películas de PS con todos estos materiales dispersados para estudiar las propiedades de emisión, centrándonos en la eficacia de las distintas estrategias para prevenir la fotodegradación. Con los compuestos con los grupos Tip se han obtenido tiempos de vida 3 veces mayores que las moléculas originales (ver Figura 3.8b), mientras que con el grupo t-Bu el efecto ha sido el contrario, la fotoestabilidad ha disminuido. En cuanto al compuesto COPV2-d_2, la fotoestabilidad solo ha sido ligeramente mayor que para el COPV2, lo que nos indica que el terminal del átomo H(D) no es el factor determinante en el proceso de degradación.

Los umbrales se han mantenido constantes dentro de cada familia teniendo en cuenta el efecto de la absorción, exceptuando al compuesto COPV1-t-Bu, que presenta un umbral mucho mayor que el resto de los derivados. Adicionalmente, todos los sustituyentes tienen el efecto adicional de modificar ligeramente la longitud de onda de emisión ASE, situándose en los rangos 385-413 nm para el COPV1 y sus derivados y en el rango 462-474 para el COPV2.

Estos derivados han sido utilizados para la fabricación de láseres con emisión en el azul en la publicación 2. Además, se sintetizó un nuevo derivado del COPV1 siguiendo esta misma estrategia para conseguir una emisión a una longitud de onda menor que el compuesto original, el compuesto COPV1(Me)-t-Bu. Este compuesto emite en 374 nm, siendo el derivado con menor longitud de onda de emisión de todos los estudiados, con lo que sirvió para comprobar las posibilidades de nuestro método experimental para fabricar dispositivos que emiten en ese rango.

Justificación de la unidad temática

En la sección anterior se han presentado los principales resultados de cada una de las publicaciones que forman la tesis. Estos resultados se encuentran englobados en al menos uno de los objetivos propuestos.

El primer objetivo hacer referencia a las publicaciones 1, 2, 3, 4 y 5, ya que todas ellas pretenden optimizar los láseres DFB. Las tres primeras publicaciones logran ese objetivo a través de la optimización del resonador, lo que resulta en: i) unos mejores

umbrales y eficiencias, por la publicación 1; ii) una extensión del rango operativo de estos dispositivos, que permiten emisión en la zona azul del espectro, por la publicación 2; y iii) la determinación del efecto de situar el resonador encima o debajo de la capa activa, por la publicación 3. Además, las publicaciones 4 y 5 se centran en la determinación del espesor y el índice de refracción de películas delgada mediante métodos espectrofotométricos no destructivos. Esto permite la caracterización precisa de todas las capas que forman un dispositivo láser DFB (capa activa y capa de DCG), optimizando el proceso de fabricación.

Las publicaciones 6, 7 y 8 se incluyen en el segundo objetivo propuesto, ya que tratan del estudio de nuevas moléculas orgánicas para ser utilizadas como material activo en TFOLs. Estas tres publicaciones analizan las propiedades de emisión de tres familias distintas de compuestos. La publicación 2 también está incluida en este objetivo, ya que presenta los dispositivos realizados con los materiales estudiados en la publicación 8 y también incluye un nuevo derivado con emisión en el UV.

Conclusiones

- **El control de los parámetros geométricos y de fabricación en los resonadores de los láseres DFB es crucial para obtener un rendimiento optimizado.** Se estudió la influencia de la capa residual y de la modulación de la red en los láseres DFB con el resonador sobre la capa activa. Los resultados mostraron que el umbral menor y la eficiencia mayor se obtuvieron en los dispositivos sin capa residual. En cuanto a la modulación, valores bajos mejoran el umbral pero disminuyen la eficiencia. Se puede alcanzar un compromiso utilizando una red con una modulación entre 100 y 130 nm: su umbral es menor a 25 μJ/cm^2 y su eficiencia alcanza el 80 % de su máximo valor. Este comportamiento se puede interpretar en términos de la superposición de la distribución del campo eléctrico y la red. Además, se ha utilizado un nuevo método de revelado seco con el plasma de oxígeno obtenido de una máquina sencilla de tratamiento de superficies, demostrando que es un método válido para obtener láseres DFB con buen rendimiento y alta calidad.

- **Los láseres DFB con resonadores de DCG encima de la capa activa han demostrado ser adecuados para la fabricación de dispositivos con emisión entre 375 y 475 nm.** No se han encontrado limitaciones de resolución ni siquiera para los periodos menores requeridos (235 nm). Además, las redes con perfil rectangular y *duty cycle* de 0.75 son muy convenientes para este tipo de dispositivos, ya que consiguen equilibrar las pérdidas y la realimentación en estos dispositivos. Estas redes optimizadas se pusieron a prueba fabricando dispositivos DFB para múltiples moléculas con emisión en el azul como material activo. Entre ellas, un nuevo derivado del COPV1, COPV1(Me)-*t*-Bu se sintetizó y caracterizó.

Este es el derivado con menor longitud de onda de emisión (374 nm), lo que extiende el uso de estos dispositivos al UV.

- **La configuración con el resonador sobre la capa activa (RT) presenta numerosas ventajas con respecto a la configuración con el resonador debajo de la capa activa (RB) en láseres DFB con resonadores de DCG.** Estas dos configuraciones fueron puestas a prueba utilizando TPD como material activo, el cual puede ser dispersado en altas cantidades en la matriz de PS. Esto provoca cambios en el índice de refracción de la capa activa y consecuentemente en el índice efectivo del dispositivo. Para altas concentraciones de TPD (> 20 wt %), ambas configuraciones presentan un umbral similar, mientras que para concentraciones menores el umbral es menor en la configuración RT debido al mejor confinamiento del campo eléctrico en la capa activa. En términos de fotoestabilidad, los dispositivos RT presentan un mejor comportamiento (valores 2 veces mayores), ya que la localización del resonador sobre la capa activa proporciona protección a la molécula ante la fotooxidación por iluminación UV.

- **El nuevo método espectrofotométrico permite medir espesores por debajo de 500 nm.** La precisión de los resultados para películas de decenas de nm con bajos índices de refracción (1.5-1.7) es comparable a la obtenida con el método de las envolventes para películas de 1 μm y con un índice de refracción de 3. Además, en el caso de los polímeros ópticos (OP), muy utilizados en el campo de los láseres orgánicos, el método permite la determinación simultánea del índice de refracción y del espesor de la película. Se analizó una colección de OPs para encontrar un comportamiento óptico general de los mismos, que permite reducir el cálculo de la dispersión espectral del índice de refracción a una única variable. Esto supone un ahorro de tiempo y trabajo al no necesitar ningún método externo para la obtención del índice de refracción. La precisión del método depende del parecido entre el índice de refracción de la capa y del sustrato. Para el caso de PS y PMMA (con índices de 1.59 y 1.49 respectivamente) depositados sobre un sustrato de FS (índice de 1.45), el espesor mínimo medible fue de unos 30 nm para el PS y 60 nm para el PMMA. Los errores en el índice y en el espesor fueron de 0.003 y 2 nm para el PS y de 0.006 y 4 nm para el PMMA.

- **Se presentan por primera vez láseres DFB basados en nanografenos. La fabricación de láseres DFB utilizando los nanografenos FZ1, FZ2 y FZ3 como materiales activos proporcionan un gran potencial para este tipo de materiales en aplicaciones láser.** Estos nanografenos derivan del antraceno y se caracterizan por tener cuatro bordes zigzag, con cambios en su mecanismo ASE conforme aumenta su tamaño molecular, con longitudes de onda ASE de 486 nm, 590 nm y 685 nm para FZ1, FZ2 y FZ3 respectivamente. Presentan una estabilidad química y ante la fotodegradación excepcional, con tiempos de vida mayores de $2 times 10^5$ pulsos para el FZ2 y FZ3. Además, fueron capaces

61

de actuar como guía de onda para láseres DFB dispersados en una concentración muy baja (1 wt %), evitando interacciones moleculares o reacciones que podrían disminuir la fotoluminiscencia, manteniendo un umbral bajo en comparación con otras moléculas orgánicas.

- **Se desarrolló la síntesis de PAH de gran tamaño sin agregación, presentando buenas características para ser utilizado en láseres orgánicos.** Fueron desarrollados a partir de perilenos y anillos CP, presentando una gran eficiencia de luminiscencia en estado sólido gracias a la supresión de las interacciones pi-pi en la periferia debido a la presencia de anillos CP. Los PAHs ZY-01 y ZY-02 presentan una estructura prácticamente plana, lo que permite que las capas de PS con estos materiales dispersos muestren ASE. Esto llevó a la fabricación de láseres DFB eficientes con longitud de onda sintonizable, centradas en 515 nm y 570 nm respectivamente. Por el contrario, ZY-03 presenta una estructura torcida y no presenta ASE ni comportamiento láser.

- **Los sustituyentes protectores Tip (2,4,3-triisopropylpheny) añadidos en las posiciones terminales del COPV1 y COPV2 han demostrado ser una buena estrategia para mejorar la fotoestabilidad ASE.** La fotoestabilidad fue 3 veces mayores en estos derivados que en las moléculas originales COPV1 y COPV2. Se intentaron otras estrategias que no fueron satisfactorias a la hora se obtener una mejora en la fotoestabilidad. Los derivados con el sustituyente tert-butyl empeoraron su fotoestabilidad y su umbral, mientras que el derivado COPV2-d_2 con átomos de deuterio en las posiciones terminales no mejoró tampoco la fotoestabilidad, probando que el átomo H en la posición terminal no es el factor determinante en este proceso. Aunque todas las estrategias probadas no sirvieron para mejorar la fotoestabilidad, sí que tuvieron un efecto secundario que puede ser explotado, como la sintonizabilidad de la longitud de onda de emisión al añadir nuevos sustituyentes. Estas longitudes de onda ASE cambiaron entre 385 nm y 413 nm para los derivados del COPV1 y entre 462 nm y 474 para los derivados del COPV2.

Publications and conference contributions

Other publications

[1] Muñoz-Mármol, R., Bonal, V., Paternò, G.M., Ross, A.M., Boj, P.G., Villalvilla, J.M., Quintana, J.A., Scotognella, F., D'Andrea, C., Sardar, S., Lanzani, G., Gu, Y., Wu, J., Díaz-García, M. A. (2020) Dual Amplified Spontaneous Emission and Lasing from Nanographene Films. *Nanomaterials*, **10**, 1525.

[2] Muñoz-Mármol, R., Gordillo, F., Bonal, V., Villalvilla, J.M., Boj, P.G., Quintana, J.A., Ross, A.M., Paternò, G.M., Scotognella, F., Lanzani, G.,Derradji, A., Sancho-García, J.C., Gu, Y., Wu, J., Casado, J., Díaz-García, M.A. (2021) Near-Infrared Lasing in Four-Zigzag Edged Nanographenes by 1D versus 2D Electronic -Conjugation. *Adv. Funct. Mater.* 2105073

[3] Paternò, G.M., Chen, Q., Muñoz-Mármol, R., Guizzardi, M., Bonal, V., Kabe, R., Barker, A., Boj, P.G., Chatterjee, S., Ie, Y., Villalvilla, J.M., Quintana, J.A., Scotognella, F., Müllen, K., Díaz-García, M.A., Narita, A., Lanzani, G. (2021) Excited States Engineering Enables Efficient Near-Infrared Lasing in Nanographenes. *Mater. Horizons*, **9**, 393.

[4] Tsuji, H., Shitomi, A., Hamaguchi, N., Egawa, Y., Bonal, V., Boj, P.G., Villalvilla, J.M., Quintana, J.A., Díaz-García, M.A. (2021) Violet-emitting distributed-feedback laser using a naphtho[2,1-b:6,5-b]difuran derivative. *J. Mater. Chem. C*, **9**, 17287–17290.

[5] Gu, Y., Muñoz-Mármol, R., Fan, W., Han, Y., Wu, S., Li, Z., Bonal, V., Villalvilla, J.M. , Quintana, J.A. , Boj, P.G. , Díaz-García, M.A., Wu, J. (2022) Peri-Acenoacene for Solution Processed Distributed Feedback Laser: The Effect of 1,2-Oxaborine Doping. *Adv. Opt. Mater.* 2022, **10**, 2102782.

Conference contributions

[1] "Latest Advances on Solution-processed Thin film Organic Lasers" (Invited Oral Communication). M. A. Díaz-García, **R. Muñoz-Mármol**, V. Bonal, M. Morales-Vidal, J. M. Villalvilla, E. M. Calzado, C. Vázquez, P. G. Boj, J. A. Quintana. 2018 Advanced Photonics Congress, July 2018, Zurich, Switzerland.

[2] "Láseres orgánicos de película delgada con resonadores difractivos poliméricos" (Oral Communication) **V. Bonal**, J. A. Quintana, J. M. Villalvilla, P. G. Boj, M. A. Díaz-García. XII Reunión Nacional de Óptica, July 2018, Castellón, Spain.

[3] "Solution-Proceed Organic Lasers with Top-Layer Nanostructured Resonators" (Oral Communication). **M. A. Díaz-García**, V. Bonal, R. Muñoz-Mármol, M. Morales-Vidal, J. M. Villalvilla, P. G. Boj y J. A. Quintana. NanoSpain 2019 Conference, May 2019, Barcelona, Spain.

[4] "Láseres con realimentación distribuida completamente orgánicos" (Poster) **V. Bonal**, J. A. Quintana, J. M. Villalvilla, P. G. Boj, M. A. Díaz-García. XI Reunión Española de Optoelectrónica, July 2019, Zaragoza, Spain

[5] "Novel Organic Compounds for Solution-Processed Thin Film Organic Lasers" (Oral Communication). **M. A. Díaz-García**, V. Bonal, R. Muñoz-Mármol, M. Morales-Vidal, J. M. Villalvilla, M. Martínez-Marco, E. M. Calzado, C. Vázquez, P. G. Boj, J. A. Quintana. 14th International Symposium on Functional -Electron Systems, July 2019, Berlin, Germany.

[6] "Effect of the device architecture in high concentration organic distributed feedback lasers" (Oral Communication) **V. Bonal**, J. A. Quintana, J. M. Villalvilla, P. G. Boj, R. Muñoz-Mármol, J. C. Mira-Martínez, M. A. Díaz-García. II Symposium on Chemical and Physical Sciences for Young Researchers, March 2022, Murcia, Spain

[7] "Latest advances in organic distributed feedback lasers with top-layer resonator" (Oral Communication) **V. Bonal**, J. A. Quintana, J. M. Villalvilla, P. G. Boj, R. Muñoz-Mármol, J. C. Mira-Martínez, M. A. Díaz-García. XXXVIII Reunión Bienal de la Real Sociedad Española de Física, July 2022, Murcia, Spain

Bibliography

[1] Hecht, J. (2010) A short history of laser development. *Opt. Eng.,* **49**(9), 091002.

[2] Einstein, A. (1917) Zur Quantentheorie der Strahlung. *Phys. Zeitschrift,* **18**, 121–128.

[3] Anni, M. and Lattante, S. (2018) Organic Lasers: Fundamentals, Developments, and Applications, Pan Stanford Publishing, Singapore.

[4] Fabrikant, V. A. (1940) Emission mechanism of a gas discharge. *Tr. VEI,* **41**, 236.

[5] Schawlow, A. L. and Townes, C. H. (1958) Infrared and optical masers. *Phys. Rev.,* **112**(6), 1940–1949.

[6] Maiman, T. H. (1960) Stimulated Optical Radiation in Ruby. *Nature,* **187**, 493–494.

[7] Dudley, J. M. (2010) Light, Lasers, and the Nobel Prize. *Adv. Photonics,* **2**(5), 050501.

[8] Siegman, A. E. (1986) Lasers, University Science Books, Mill Valley, California.

[9] Milonni, P. W. and Eberly, J. H. (2010) Laser physics, John Wiley and Sons, Hoboken, New Jersey.

[10] Rullière, C. and Alfano, R. R. (2005) Femtosecond Laser Pulses: Principles and Experiments, Springer, New York, NY.

[11] Svelto, O. (2010) Principles of Lasers, Springer, New York, NY 5th edition.

[12] Milanese, S., de Giorgi, M. L., and Anni, M. (2020) Determination of the best empiric method to quantify the amplified spontaneous emission threshold in polymeric active waveguides. *Molecules,* **25**(13), 2992.

[13] Lifante, G. (2003) Integrated Photonics, Vol. 90, Wiley, Chichester, England.

[14] Boudrioua, A. (2009) Photonic Waveguides: Theory and Applications, Wiley, London.

[15] Samuel, I. D. W. and Turnbull, G. A. (2007) Organic Semiconductor Lasers. *Chem. Rev.,* **107**, 1272–1295.

[16] Chénais, S. and Forget, S. (2012) Recent advances in solid-state organic lasers. *Polym. Int.,* **61**(3), 390–406.

[17] Grivas, C. and Pollnau, M. (2012) Organic solid-state integrated amplifiers and lasers. *Laser Photon. Rev.,* **462**(4), 419–462.

[18] Kuehne, A. J. C. and Gather, M. C. (2016) Organic Lasers : Recent Developments on Materials , Device Geometries , and Fabrication Techniques. *Chem. Rev.,* **116**(21), 12823–12864.

[19] Kogelnik, H. and Shank, C. V. (1972) Coupled-wave theory of distributed feedback lasers. *J. Appl. Phys.,* **43**(5), 2327–2335.

[20] Jiang, Y., Liu, Y.-Y., Liu, X., Lin, H., Gao, K., Lai, W.-Y., and Huang, W. (2020) Organic solid-state lasers: a materials view and future development. *Chem. Soc. Rev.,* **49**(16), 5885–5944.

[21] Sorokin, P. P. and Lankard, J. R. (1966) Stimulated Emission Observed from an Organic Dye, Chloro-aluminum Phthalocyanine. *IBM J. Res. Dev.,* **10**(2), 162–163.

[22] Schäfer, F. P., Schmidt, W., and Volze, J. (1966) Organic dye solution laser. *Appl. Phys. Lett.,* **9**(8), 306–309.

[23] Yang, Y., Turnbull, G. A., and Samuel, I. D. (2008) Hybrid optoelectronics: A polymer laser pumped by a nitride light-emitting diode. *Appl. Phys. Lett.,* **92**(16), 92–95.

[24] Gather, M. C. and Yun, S. H. (2011) Single-cell biological lasers. *Nat. Photonics,* **5**(7), 406–410.

[25] Sandanayaka, A. S. D., Matsushima, T., Bencheikh, F., Terakawa, S., Potscavage, W. J., Qin, C., Fujihara, T., Goushi, K., Ribierre, J.-C., and Adachi, C. (2019) Indication of current-injection lasing from an organic semiconductor. *Appl. Phys. Express,* **12**(6), 061010.

[26] Muñoz-Mármol, R., Zink-Lorre, N., Villalvilla, J. M., Boj, P. G., Quintana, J. A., Vázquez, C., Anderson, A., Gordon, M. J., Sastre-Santos, A., Fernández-Lázaro, F., and Díaz-García, M. A. (2018) Influence of Blending Ratio and Polymer Matrix on the Lasing Properties of Perylenediimide Dyes. *J. Phys. Chem. C,* **122**, 24896–24906.

[27] Brütting, W. and Adachi, C., (eds.) (2012) Physics of Organic Semiconductors, Wiley-VCH Verlag, Weinheim, Germany.

[28] Hide, F., Díaz-García, M. A., Schwartz, B. J., Andersson, M. R., Pei, Q., and Heeger, A. J. (1996) Semiconducting polymers: A new class of solid-state laser materials. *Science,* **273**(5283), 1833–1836.

[29] Tessler, N., Denton, G. J., and Friend, R. H. (1996) Lasing from conjugated-polymer microcavities. *Nature,* **382**, 695–697.

[30] Geerts, Y. and Müllen, K. (1999) Advanced Light Emitting Dyes: Monomers, Oligomers, and Polymers. In *Appl. Fluoresc. Chem. Biol. Med.* pp. 299–324 Springer-Verlag Berlin Heidelberg.

[31] Morales-Vidal, M., Boj, P. G., Villalvilla, J. M., Quintana, J. A., Yan, Q., Lin, N. T., Zhu, X., Ruangsupapichat, N., Casado, J., Tsuji, H., Nakamura, E., and Díaz-García, M. A. (2015) Carbon-bridged oligo(p-phenylenevinylene)s for photostable and broadly tunable, solution-processable thin film organic lasers. *Nat. Commun.,* **6**, 8458.

[32] Zhu, X., Tsuji, H., López Navarrete, J. T., Casado, J., and Nakamura, E. (2012) Carbon-Bridged Oligo(phenylenevinylene)s: Stable π-Systems with High Responsiveness to Doping and Excitation. *J. Am. Chem. Soc.,* **134**(46), 19254–19259.

[33] Burrezo, P. M., Lin, N.-T., Nakabayashi, K., Ohkoshi, S.-i., Calzado, E. M., Boj, P. G., Díaz García, M. A., Franco, C., Rovira, C., Veciana, J., Moos, M., Lambert, C., López Navarrete, J. T., Tsuji, H., Nakamura, E., and Casado, J. (2017) Bis(aminoaryl) Carbon-Bridged Oligo(phenylenevinylene)s Expand the Limits of Electronic Couplings. *Angew. Chemie Int. Ed.,* **56**(11), 2898–2902.

[34] Tsuji, H. and Nakamura, E. (2019) Carbon-Bridged Oligo(phenylene vinylene)s: A de Novo Designed, Flat, Rigid, and Stable π-Conjugated System. *Acc. Chem. Res.,* **52**(10), 2939–2949.

[35] Burrezo, P. M., Zhu, X., Zhu, S.-F., Yan, Q., López Navarrete, J. T., Tsuji, H., Nakamura, E., and Casado, J. (2015) Planarization, Fusion, and Strain of Carbon-Bridged Phenylenevinylene Oligomers Enhance π-Electron and Charge Conjugation: A Dissectional Vibrational Raman Study. *J. Am. Chem. Soc.,* **137**(11), 3834–3843.

[36] Novoselov, K. S., Geim, A. K., Morozov, S. V., Jiang, D., Zhang, Y., Dubonos, S. V., Grigorieva, I. V., and Firsov, A. A. (2004) Electric Field Effect in Atomically Thin Carbon Films. *Science,* **306**(5696), 666–669.

[37] Wang, X.-Y., Yao, X., and Müllen, K. (2019) Polycyclic aromatic hydrocarbons in the graphene era, Vol. 62, , .

[38] Wu, J., Pisula, W., and Mu, K. (2007) Graphenes as Potential Material for Electronics. *Chem. Rev.,* **107**(3), 718–747.

[39] Narita, A., Wang, X. Y., Feng, X., and Müllen, K. (2015) New advances in nanographene chemistry. *Chem. Soc. Rev.,* **44**(18), 6616–6643.

[40] Segawa, Y., Ito, H., and Itami, K. (2016) Structurally uniform and atomically precise carbon nanostructures. *Nat. Rev. Mater.,* **1**(1), 15002.

[41] Kastler, M., Pisula, W., Wasserfallen, D., Pakula, T., and Müllen, K. (2005) Influence of alkyl substituents on the solution- and surface-organization of hexa-peri-hexabenzocoronenes. *J. Am. Chem. Soc.,* **127**(12), 4286–4296.

[42] Ritter, K. A. and Lyding, J. W. (2009) The influence of edge structure on the electronic properties of graphene quantum dots and nanoribbons. *Nat. Mater.,* **8**(3), 235–242.

[43] Rieger, R. and Müllen, K. (2010) Forever young: Polycyclic aromatic hydrocarbons as model cases for structural and optical studies. *J. Phys. Org. Chem.,* **23**(4), 315–325.

[44] Paternò, G. M., Chen, Q., Wang, X. Y., Liu, J., Motti, S. G., Petrozza, A., Feng, X., Lanzani, G., Müllen, K., Narita, A., and Scotognella, F. (2017) Synthesis of Dibenzo[hi,st]ovalene and Its Amplified Spontaneous Emission in a Polystyrene Matrix. *Angew. Chemie - Int. Ed.,* **56**(24), 6753–6757.

[45] Muñoz-Mármol, R., Bonal, V., Paternò, G. M., Ross, A. M., Boj, P. G., Villalvilla, J. M., Quintana, J. A., Scotognella, F., D'Andrea, C., Sardar, S., Lanzani, G., Gu, Y., Wu, J., and Díaz-García, M. A. (2020) Dual Amplified Spontaneous Emission and Lasing from Nanographene Films. *Nanomaterials,* **10**(8), 1525.

[46] Muñoz-Mármol, R., Gordillo, F., Bonal, V., Villalvilla, J. M., Boj, P. G., Quintana, J. A., Ross, A. M., Paternò, G. M., Scotognella, F., Lanzani, G., Derradji, A., Sancho-García, J. C., Gu, Y., Wu, J., Casado, J., and Díaz-García, M. A. (2021) Near-Infrared Lasing in Four-Zigzag Edged Nanographenes by 1D versus 2D Electronic π-Conjugation. *Adv. Funct. Mater.,* p. 2105073.

[47] Paternò, G. M., Chen, Q., Muñoz-Mármol, R., Guizzardi, M., Bonal, V., Kabe, R., Barker, A., Boj, P. G., Chatterjee, S., Ie, Y., Villalvilla, J. M., Quintana, J. A., Scotognella, F., Muellen, K., Diaz-Garcia, M. A., Narita, A., and Lanzani, G. (2021) Excited States Engineering Enables Efficient Near-Infrared Lasing in Nanographenes. *Mater. Horizons,* **9**(1), 393.

[48] Gu, Y., Muñoz-Mármol, R., Fan, W., Han, Y., Wu, S., Li, Z., Bonal, V., Villalvilla, J. M., Quintana, J. A., Boj, P. G., Díaz-García, M. A., and Wu, J. (2022) Peri-Acenoacene for Solution Processed Distributed Feedback Laser : The Effect of 1,2-Oxaborine Doping. *Adv. Opt. Mater.,* **10**(7), 2102782.

[49] Quintana, J. A., Villalvilla, J. M., Morales-Vidal, M., Boj, P. G., Zhu, X., Ruangsupapichat, N., Tsuji, H., Nakamura, E., and Díaz-García, M. A. (2017) An Efficient and Color-Tunable Solution-Processed Organic Thin-Film Laser with a Polymeric Top-Layer Resonator. *Adv. Opt. Mater.,* **5**(19), 1700238.

[50] Ramírez, M. G., Morales-Vidal, M., Navarro-Fuster, V., Boj, P. G., Quintana, J. A., Villalvilla, J. M., Retolaza, A., Merino, S., and Díaz-García, M. A. (2013) Improved performance of perylenediimide-based lasers. *J. Mater. Chem. C,* **1**(6), 1182–1191.

[51] Ramirez, M. G., Boj, P. G., Navarro-Fuster, V., Vragovic, I., Villalvilla, J. M., Alonso, I., Trabadelo, V., Merino, S., and Díaz-García, M. A. (2011) Efficient organic distributed feedback lasers with imprinted active films. *Opt. Express,* **19**(23), 22443–22454.

[52] Calzado, E. M., Villalvilla, J. M., Boj, P. G., Quintana, J. A., and Díaz-García, M. A. (2006) Concentration dependence of amplified spontaneous emission in organic-based waveguides. *Org. Electron.,* **7**(5), 319–329.

[53] Manifacier, J. C., Gasiot, J., and Fillard, J. P. (1976) A simple method for the determination of the optical constants n, k and the thickness of a weakly absorbing thin film. *J. Phys. E.,* **9**, 1002–1004.

[54] Swanepoel, R. (1983) Determination of the thickness and optical constants of amorphous silicon. *J. Phys. E.,* **16**, 1214–1222.

[55] Swanepoel, R. (1985) Determining refractive index and thickness of thin films from wavelength measurements only. *J. Opt. Soc. Am. A,* **2**(8), 1339–1343.

[56] Poelman, D. and Smet, P. F. (2003) Methods for the determination of the optical constants of thin films from single transmission measurements: a critical review. *J. Phys. D. Appl. Phys.,* **36**, 1850–1857.

[57] Minkov, D. A., Gavrilov, G. M., Angelov, G. V., Moreno, J. M., Vázquez, C. G., Ruano, S. M., and Márquez, E. (2018) Optimisation of the envelope method for characterisation of optical thin film on substrate specimens from their normal incidence transmittance spectrum. *Thin Solid Films,* **645**, 370–378.

[58] Sultanova, N. G., Kasarova, S. N., and Nikolov, I. D. (2013) Characterization of optical properties of optical polymers. *Opt. Quantum Electron.,* **45**(3), 221–232.

[59] Kasarova, S., Sultanova, N., Petrova, T., Dragostinova, V., and Nikolov, I. (2009) Refractive characteristics of thin polymer films. *J. Optoelectron. Adv. Mater.,* **11**(10), 1440–1443.